Single-cell immune profiling of atherosclerosis: from omics to therapeutics

Depuydt, M.A.C.

Chapter 3

Microanatomy of the human atherosclerotic plaque by single-cell transcriptomics

Circulation Research 2020; 127:1437-1455

Marie A.C. Depuydt[1#], Koen H.M. Prange[2#], Lotte Slenders[3#], Tiit Örd[4], Danny Elbersen[5], Arjan Boltjes[3], Saskia C.A. de Jager[5], Folkert W. Asselbergs[3], Gert J. de Borst[6], Einari Aavik[4], Tapio Lönnberg[7], Esther Lutgens[2,8], Christopher K. Glass[9,10], Hester M. den Ruijter[11], Minna U. Kaikkonen[4], Ilze Bot[1], Bram Slütter[1], Sander W. van der Laan[3], Seppo Yla-Herttuala[4], Michal Mokry[3,11*], Johan Kuiper[1*], Menno P.J. de Winther[2,8*], Gerard Pasterkamp[3*]

1. Leiden Academic Centre for Drug Research, Division of Biotherapeutics, Leiden University, The Netherlands
2. Amsterdam University Medical Centers – location AMC, University of Amsterdam, Experimental Vascular Biology, Department of Medical Biochemistry, Amsterdam Cardiovascular Sciences, Amsterdam Infection and Immunity, The Netherlands
3. Laboratory of Clinical Chemistry and Haematology, University Medical Center, The Netherlands.
4. A.I.Virtanen Institute for Molecular Sciences, University of Eastern Finland, Finland
5. Laboratory for Experimental Cardiology, University Medical Center Utrecht, The Netherlands
6. Department of Vascular Surgery, University Medical Centre Utrecht, Heidelberglaan 100, Utrecht, The Netherlands
7. Turku Bioscience Centre, University of Turku and Åbo Akademi University, 20520 Turku, Finland
8. Institute for Cardiovascular Prevention (IPEK), Munich, Germany & German Center for Cardiovascular Research (DZHK), partner site Munich Heart Alliance, Munich, Germany
9. Cell and Molecular Medicine, University of California San Diego, San Diego, CA, USA
10. School of Medicine, University of California San Diego, San Diego, CA, USA
11. Department of Cardiology, University Medical Center Utrecht The Netherlands

#These authors contributed equally; *Shared last authors

Abstract

Rationale: Atherosclerotic lesions are known for their cellular heterogeneity, yet the molecular complexity within the cells of human plaques have not been fully assessed.

Objective: Using single-cell transcriptomics and chromatin accessibility we gained a better understanding of the pathophysiology underlying human atherosclerosis.

Methods and Results: We performed single-cell RNA and single-cell ATAC sequencing on human carotid atherosclerotic plaques to define the cells at play and determine their transcriptomic and epigenomic characteristics. We identified 14 distinct cell populations including endothelial cells, smooth muscle cells, mast cells, B cells, myeloid cells, and T cells and identified multiple cellular activation states and suggested cellular interconversions. Within the endothelial cell population we defined subsets with angiogenic capacity plus clear signs of endothelial to mesenchymal transition. $CD4^+$ and $CD8^+$ T cells showed activation-based subclasses, each with a gradual decline from a cytotoxic to a more quiescent phenotype. Myeloid cells included two populations of pro-inflammatory macrophages showing IL1B or TNF expression as well as a foam cell-like population expressing TREM2 and displaying a fibrosis-promoting phenotype. ATACseq data identified specific transcription factors associated with the myeloid subpopulation and T cell cytokine profiles underlying mutual activation between both cell types. Finally, cardiovascular disease susceptibility genes identified using public GWAS data were particularly enriched in lesional macrophages, endothelial and smooth muscle cells.

Conclusion: This study provides a transcriptome-based cellular landscape of human atherosclerotic plaques and highlights cellular plasticity and intercellular communication at the site of disease. This detailed definition of cell communities at play in atherosclerosis will facilitate cell-based mapping of novel interventional targets with direct functional relevance for the treatment of human disease.

Key words: atherosclerosis, single-cell RNA sequencing, single-cell ATAC sequencing, GWAS

Non-standard Abbreviations and Acronyms.

CVD	cardiovascular disease
GWAS	genome-wide association studies
CyTOF	cytometry by time of flight
scRNA-seq	single cell RNA sequencing
scATAC-seq	single cell ATAC sequencing
FACS	fluorescence-activated cell sorting
SMC	smooth muscle cell
EndoMT	endothelial to mesenchymal transition
MACE	major adverse cardiovascular events
TF	transcription factor
(ox)LDL	(oxidized) low-density lipoprotein
DC	dendritic cell
EC	endothelial cell
CAD	coronary artery disease
DEG	differentially expressed gene
LoF	loss-of-function

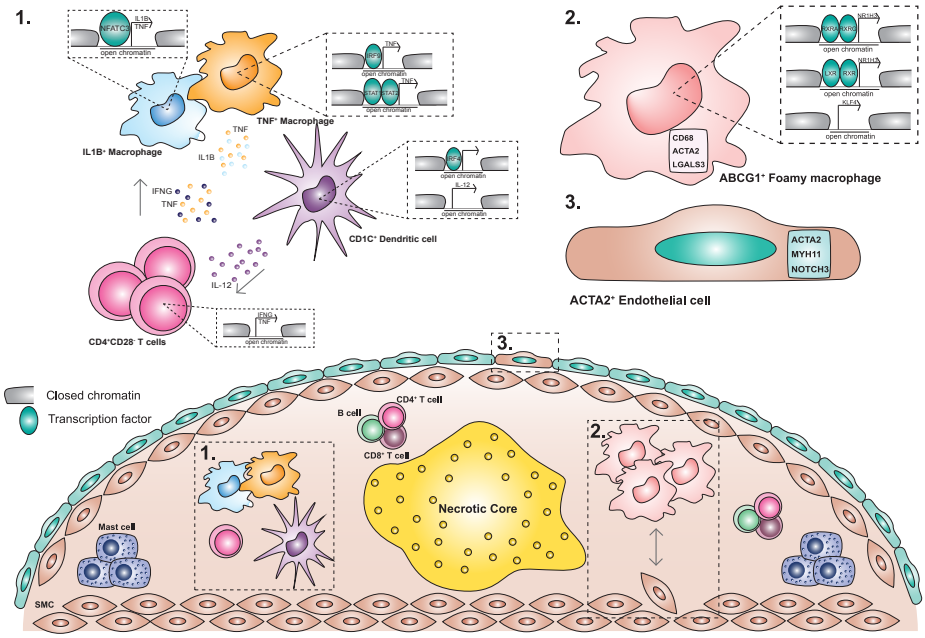

Graphical Abstract. Microanatomy of the human atherosclerotic plaque through scRNA-seq and scATAC-seq. Schematic overview of the retrieved cells in the human plaque, highlighting the local inflammation as found through the IL12-IFNγ axis between dendritic cells, $CD4^+CD28^-$ T cells and macrophages (1); the LXR_RXR induced foam cell phenotype (2) and the cellular plasticity in the plaque as seen by the $ACTA2^+$ macrophages and the $ACTA2^+$ endothelial cells that potentially undergo EndoMT .

Novelty and significance

What is known?

- Atherosclerotic lesions show a complex cellular composition that has mainly been studied using selected marker molecules
- The benefit of using single-cell RNA sequencing as unbiased method has been shown for immune cells in both murine and human atherosclerosis

What new information does this article contribute?

- Single-cell RNA sequencing of a broad cohort of human carotid plaques now provides a detailed cellular atlas of the various cell types and their phenotypes, including different clusters of endothelial and smooth muscle cells.
- Chromatin accessibility of macrophages and T cells is mapped at a single cell level and identifies relevant transcription factor binding sites.
- Mapping of cardiovascular susceptibility genes identified by GWAS to cellular subsets identifies potential cell specific targets.

It is important to determine the exact cell (sub)types and their interactions at play in atherosclerosis in order to devise novel therapeutic strategies. Here, we describe the total cellular composition of atherosclerotic plaques taken from carotid arteries of a broad cohort of patients. Our data suggests that the main immune cell subset consists of T cells, which can be subdivided by activation status. Macrophages are found in distinct populations with diverse activation patterns, inflammatory status, and foam cell characteristics. We shed light on plaque endothelial and smooth muscle cell gene expression and show cell clusters with gene expression patterns pointing towards characteristics of endothelial to mesenchymal transition. To further investigate the dynamic intra-plaque niche, we assessed ligand-receptor interactions driving our cell communities and investigated potential transcription factor activity underlying myeloid and T cell populations in the plaque by studying chromatin accessibility at the single cell level. Finally, we identified cell types enriched for cardiovascular susceptibility genes by integrating available GWAS data. Together, our data provide an in-depth map of the human atherosclerotic plaque and give valuable insights into cell types, pathways, and genes that are relevant for future research aiming at the development of novel therapeutic strategies.

Introduction

Atherosclerosis is characterized by chronic, lipid-driven vascular inflammation and is the main underlying cause of cardiovascular disease (CVD).[1] Many studies have defined cellular profiles of human atherosclerosis based on single or several marker proteins, but detailed description of the cells involved in the pathophysiology of atherogenesis is lacking. Moreover, genome-wide association studies (GWAS) have identified many loci associated with increased risk for CVD, but the translation of these findings into new therapies[2] has been hampered by the lack of information on specific cell communities in atherosclerotic plaques and the cell-specific expression patterns of druggable candidate genes at the site of disease. Recently, the immune cell composition of murine and human aortic atherosclerotic plaques has been described using cytometry by time of flight (CyTOF) and single cell RNA sequencing (scRNA-seq).[3-7] Yet, the full cellular composition of human carotid plaques, including non-immune cells, remains elusive. Therefore, we performed scRNA-seq and single-cell ATAC sequencing (scATAC-seq) on advanced human atherosclerotic plaques obtained during carotid endarterectomy and report a comprehensive overview of the various cell types in plaques and their activation status, which reveals an active, ongoing inflammation and multiple cellular interactions as well as cellular plasticity with respect to endothelial cells and macrophages. In addition, we identified cell type specific expression of GWAS risk loci for CVD.

Methods

Please see the Online Data Supplement for detailed methods.

Results

Single-cell RNA sequencing identifies 14 distinct cell populations in human atherosclerotic plaques

To examine the transcriptome of human atherosclerotic plaques, carotid endarterectomy tissue from 18 patients (77% male sex) was enzymatically digested, viable nucleated cells were isolated by fluorescence-activated cell sorting (FACS) (**Figure 1A**, **Online Figure 1A**, **Online Table 1**) and scRNA-seq libraries were prepared. After filtering cells based on the number of reported genes (see online methods), we applied unbiased clustering on 3282 cells, identifying 14 cell populations (**Figure 1B**, **C**, **Online Table 2**). Correlation of our scRNA-seq data with bulk RNA-seq

data (**Online Figure 1B**) and examining inter-patient variation of cluster distribution (**Online Figure 1C**) and size (**Online Figure 1D**) confirmed uniformity of the data except for patient 1. We assigned a cell type to each cluster based on differential expression of established lineage markers (**Figure 1B, D**). Cluster composition did not differ between sexes (**Online Figure 1E**) and cluster identities were confirmed by correlation with bulk RNA-seq datasets (**Figure 1E**).[8] We observed three non-immune cell clusters (clusters 8, 9 and 10; expressing *CD34* and *ACTA2*)[9,10] and eleven leukocyte clusters (**Figure 1B, D**). The latter included five lymphocyte clusters (clusters 0, 1, 3, 4, and 11; expressing *CD3E*, *CD4*, *CD8*, *CD79A*)[11,12], five myeloid clusters (clusters 5, 6, 7, 12 and 13; expressing *CD14*, *CD68*, *KIT*)[13–16], and one cluster containing a mixture of cells (cluster 2), which did not show a clear cell type-defining expression profile, but had similar gene expression levels as other clusters and seemed to mainly contain apoptotic myeloid and T cells (**Figure 1B, D, Online Figure 2A-D**). T cells appeared to be the most abundant population in our data set, encompassing 52.4% of all analyzed cells, whereas the myeloid populations represented 18.5% of all cells (**Online Figure 2E**). Histological analysis of matched samples confirmed that $CD3^+$ T cells indeed outnumbered the $CD68^+$ cells, which represent macrophages and to a limited extend smooth muscle cells[17], in the studied samples (number of $CD3^+$ T cells: 1880±449 vs. number of $CD68^+$ cells: 870±135) (**Online Figure 2F**).

ECs exhibited a gene expression profile indicative of activation and potential transdifferentiation

Endothelial cells were represented by cluster 9; expressing *COL4A1*, COL4A2, *SPARCL1*, and *PLVAP*, and cluster 10; expressing *MPZL2*, *SULF1*, *VWF*, and *EDN1* (**Figure 1B**, **C**, **Online Table** 2). Isolating and reclustering these clusters revealed four distinct subclasses (E.0-E.3, **Figure 2A**, **Online Table 2**). We could assign endothelial cell phenotypes to the subclasses by assessing marker genes (**Figure 2B**). E.0, E.1, and E.2 displayed classical endothelial markers *CD34* and *PECAM1*, and the vascular endothelial marker *TIE1*. E.0 showed distinct expression of *ACKR1*, which has been associated with venous endothelial cells and the vasa vasorum in mice[18,19] and *PRCP*[20], involved in angiogenesis and regeneration of damaged endothelium (**Figure 2B, C**). E.1 and E.2 separated on expression of extracellular matrix genes in E.1 and cell mobility markers *FGF18* and *HEG1* in E.2. Both populations expressed *VCAM1* (**Figure 2C**), which is expressed by activated endothelium and facilitates adhesion and transmigration of leukocytes such as monocytes and T cells.[21] Together, this suggests that E.0, E.1, and E.2 represent activated endothelium which actively aggravate inflammation in the advanced lesion by cell adhesion and neovascularization and mediating leukocyte extravasation.[22] Of note, subclass E.3 expressed typical smooth muscle cell markers such as *ACTA2*, *NOTCH3*, and *MYH11* next to the aforementioned endothelial markers

(**Figure 2C**). This, combined with its clustering among the endothelial cell clusters and enrichment of transitory and SMC related pathways (**Figure 2D**) indicated that this subset may be undergoing endothelial to mesenchymal transition (EndoMT) or vice-versa. To validate these findings we looked into the expression of ACTA2 and CD34 on sequential histological slides. **Figure 2E** shows cells lining the intraplaque vasculature that show overlapping expression.

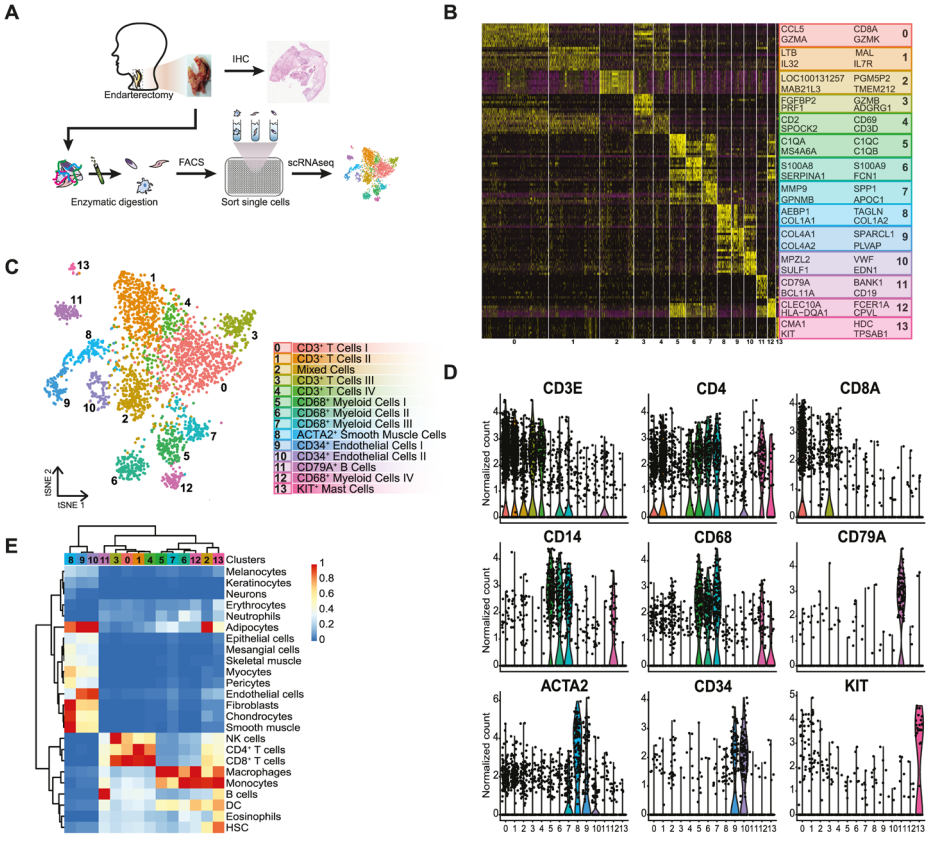

Figure 1. CCA clustering and tSNE visualization revealed 14 distinct populations. A) Experimental setup: plaque samples obtained from endarterectomy procedures were digested, single viable cells were FACS sorted in a PCR plate, and CEL-seq2 was performed. B) Heatmap of top marker genes per cluster. C) tSNE visualization of clustering revealed 14 cell populations. Population identities were determined based on marker gene expression. D) Violin plots of signature genes confirmed population identities, as well as E) by similarity to known cell type in reference RNA-seq data sets.

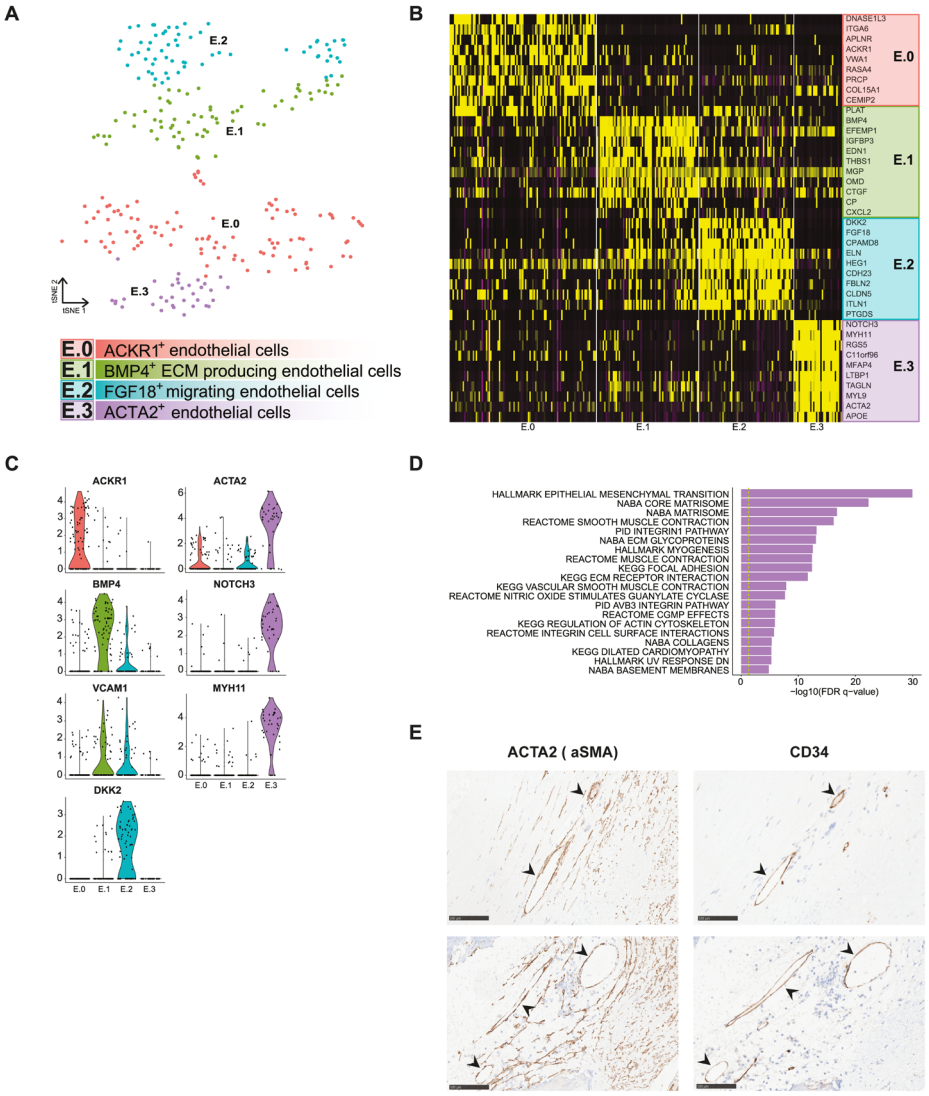

Figure 2. Subclustering of endothelial cells revealed 4 distinct populations. A) tSNE visualization of clustering revealed 4 distinct endothelial cell populations. B) Heatmap of top marker genes per cluster. C) Violin plots of endothelial cell-specific markers, genes involved in endothelial cell angiogenesis and activation and genes that are associated with EndoMT. D) Top pathways associated with cluster E.3. E) Examples of ACTA2 and CD34 expression in a monolayer of cells lining intraplaque vasculature on sequential histological slides of two different patients. Scale bars represent 100µm.

Synthetic phenotype dominates in plaque smooth muscle cells

Smooth muscle cells were represented by cluster 8; expressing *MYH11*, *PDGFRB*, *NOTCH3* and *MFAP4*[23-25] (**Figure 1B**, **C**, **Online Table 2**), which separated into two subclasses (**Online Figure 3A**): a cluster of SMCs with contractile characteristics (cluster S.1; expressing *MYH11*, *ACTA2* and *TAGLN*), and a cluster of synthetic-like SMCs (cluster S.0; expressing *COL1A1*, *MGP* and *COL3A1*)[26] (**Online Figure 3B**, **C**, **Online Table 2**). The low expression of typical SMC markers in cluster S.0 and upregulation of extracellular matrix genes suggested that a subset of these cells were derived from the established cap portion of the plaque. A limited number of cells within this cluster was *KLF4*$^{+}$ (**Online Figure 3D**), indicative of differentiation from vascular smooth muscle cells into either a synthetic or macrophage-like phenotype.

Intraplaque T cells are defined by activation status

Lymphocyte clusters consisted of one small, but homogenous cluster of B cells (cluster 11; expressing *CD79A*, *FCER2*, *CD22* and *CD79B*)[27-29] (**Figure 1B**, **C**, **Online Table 2**), and four T cell clusters. To define the T cells in more detail, we assessed the CD4^{+} T cells (expression *CD4* > *CD8*) and the CD8^{+} T cells (expression *CD8* > *CD4*) from *CD3* enriched clusters 0, 1, 3 and 4. Isolating and reclustering the CD4^{+} T cells revealed five subclasses (CD4.0-CD4.4, **Figure 3A**, **Online Table 2**) of which the primary difference was their activation state rather than the transcription factors and cytokines commonly used to define CD4^{+} T helper subsets (Figure 3B, C). CD4.0 and CD4.1 exerted a cytotoxic gene expression profile exemplified by expression of *GZMA*, *GZMK* and *PRF1*. Apart from these cytotoxic transcripts, cells in CD4.0 also showed very little *CD28* expression and some *GZMB* expression, suggesting that these cells are cytotoxic CD4^{+}CD28^{null} cells, that have previously been correlated with unstable angina and increased risk of Major Adverse Cardiovascular Events (MACE).[30,31] In addition, gene expression in this cluster confirmed an enrichment in pro-inflammatory pathways associated with adaptive immune responses (**Figure 3D**). Using flow cytometry, we confirmed the cytotoxic character of the CD4^{+}CD28^{null} cells, which showed that significantly more CD4^{+}CD28^{-} cells contained granzyme B as compared to the CD4^{+}CD28^{+} cells (**Figure 3E**, **Online Figure 4A**). CD4.2 and CD4.4 were characterized by expression of *IL7R, LEF1* and *SELL*, associated with a naïve and central-memory phenotype. The final CD4^{+} subclass (CD4.3) was identified as a regulatory T cell cluster based on the expression of the classical markers *FOXP3*, *IL2RA* (CD25) and *CTLA4*[32] (**Figure 3B**, **Online Table 2**). Interestingly, we also found some co-expression of FOXP3 with transcription factors RORA and GATA3 in this cluster (**Online Figure 4B**), which has respectively been associated with the enhanced immunosuppressive function of regulatory T cells[33] and with the prevention of polarization towards other T_H subsets[34]. Expression of the T helper (T_H) cell subset-

specific transcription factors *TBX21* (Tbet; Th1), *GATA3* (Th2) and *RORC* (RORγT; Th17) was not linked to a specific cluster (Online Figure 4C), which seems to be a common phenomenon when dealing with T cell scRNA-seq data.[35,36] By analyzing the CD4$^+$ T cells in a clustering-independent method by selecting all cells that have the expression of both CD3E and CD4 and subsequently analyzing the expression of single T_H specific transcription factors we find that a large population of T cells did not express a clear signal of the transcription factors (**Online Figure 4D**).

Analysis of CD8$^+$ T cells revealed three subclasses (**Online Figure 5A**, **B**), which were similarly to CD4$^+$ T cells defined by differences in activation state. CD8.0 was identified as an effector-memory subset, characterized by expression of *GZMK*, *GZMA*, and *CD69*, indicating recent T cell receptor activity (**Online Figure 5C**). A clear, terminally differentiated, cytotoxic CD8$^+$ T cell profile was observed in CD8.1, which showed expression of *GZMB*, *TBX21*, *NKG7*, *GNLY*, *ZNF683* and *CX3CR1* and in line, this subclass lacked *CD69* expression. Finally, CD8.2 displayed a quiescent, central-memory CD8$^+$ T cell phenotype with expression of *LEF1*, *SELL*, *IL7R* and *LTB*. In contrast to Fernandez *et al*.[7] and previous scRNA-seq data obtained from various cancers, we did not detect a clear exhausted phenotype in the CD8$^+$ T cells.[35-37] The CD8 clusters with reduced cytotoxic potential show expression of *CD69* suggesting recent TCR activation and it will be of future interest to examine how these CD8$^+$ populations were activated and how they affect the pathogenesis of atherosclerosis. This could indicate that not the cytotoxic, but the more quiescent CD8$^+$ T cell-subsets are responding to plaque-specific antigens and may be more relevant in the pathogenesis of atherosclerosis. Using experimental mouse models of atherosclerosis it has been shown that the majority of CD8$^+$ T cells in the plaque are antigen-specific[38], but so far little is known regarding the plaque-antigen(s) they respond to. Whereas CD4$^+$ T cells have been shown to respond to (ox)LDL and its related apoB100 peptide, plaque-antigen(s) for CD8$^+$ remain mostly indefinable.[39] Therefore, we are unable to define which antigens have activated the T cells in the atherosclerotic lesion.

Figure 3. Subclustering of CD4$^+$ T cells revealed 5 distinct populations. A) tSNE visualization of clustering revealed 5 distinct CD4$^+$ T cell populations. B) Dotplot of cluster-identifying genes and T cell transcription factors. C) Violin plots of CD4.0 characterizing cytotoxic genes. D) Flow cytometry analysis of Granzyme B production by CD4$^+$CD28$^-$ cells on defrosted plaque samples. E). Top pathways associated with cluster CD4.0. Data shown as mean±SD (n = 10; obtained from cohort 1 and 2). *p<0.05. ►

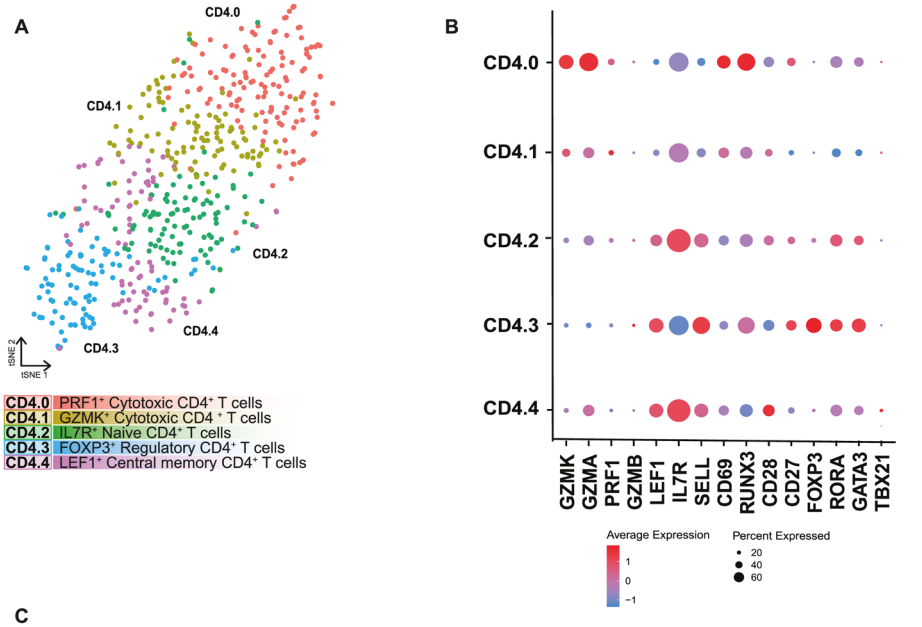
A
CD4.0
CD4.1
CD4.2
CD4.3
CD4.4
tSNE 2
tSNE 1
CD4.0 PRF1+ Cytotoxic CD4+ T cells
CD4.1 GZMK+ Cytotoxic CD4 + T cells
CD4.2 IL7R+ Naive CD4+ T cells
CD4.3 FOXP3+ Regulatory CD4+ T cells
CD4.4 LEF1+ Central memory CD4+ T cells
B
CD4.0
CD4.1
CD4.2
CD4.3
CD4.4
GZMK
GZMA
PRF1
GZMB
LEF1
IL7R
SELL
CD69
RUNX3
CD28
CD27
FOXP3
RORA
GATA3
TBX21
Average Expression
1
0
−1
Percent Expressed
20
40
60

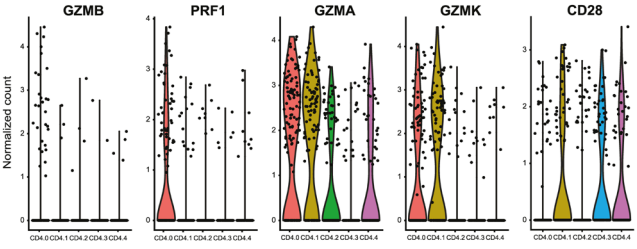
C
GZMB
PRF1
GZMA
GZMK
CD28
Normalized count
CD4.0 CD4.1 CD4.2 CD4.3 CD4.4

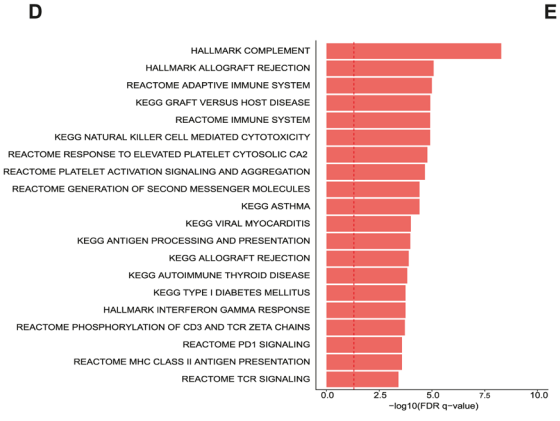
D
HALLMARK COMPLEMENT
HALLMARK ALLOGRAFT REJECTION
REACTOME ADAPTIVE IMMUNE SYSTEM
KEGG GRAFT VERSUS HOST DISEASE
REACTOME IMMUNE SYSTEM
KEGG NATURAL KILLER CELL MEDIATED CYTOTOXICITY
REACTOME RESPONSE TO ELEVATED PLATELET CYTOSOLIC CA2
REACTOME PLATELET ACTIVATION SIGNALING AND AGGREGATION
REACTOME GENERATION OF SECOND MESSENGER MOLECULES
KEGG ASTHMA
KEGG VIRAL MYOCARDITIS
KEGG ANTIGEN PROCESSING AND PRESENTATION
KEGG ALLOGRAFT REJECTION
KEGG AUTOIMMUNE THYROID DISEASE
KEGG TYPE I DIABETES MELLITUS
HALLMARK INTERFERON GAMMA RESPONSE
REACTOME PHOSPHORYLATION OF CD3 AND TCR ZETA CHAINS
REACTOME PD1 SIGNALING
REACTOME MHC CLASS II ANTIGEN PRESENTATION
REACTOME TCR SIGNALING
0.0
2.5
5.0
7.5
10.0
−log10(FDR q−value)

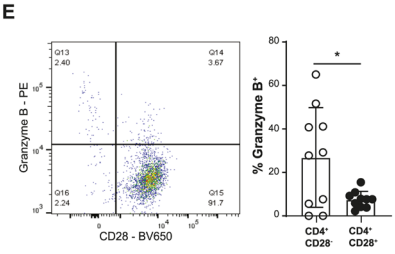
E
Granzyme B - PE
CD28 - BV650
Q13
2.40
Q14
3.67
Q16
2.24
Q15
91.7
% Granzyme B+
CD4+ CD28-
CD4+ CD28+
*

Both pro- and anti-inflammatory macrophage populations reside in the plaque

Atherosclerotic myeloid cells were represented by five clusters. A small, distinct mast cell population was defined by expression of *HDC*, *KIT*, *CMA1* and *TPSAB1*.[40] The remaining myeloid clusters, cluster 6, 7, 8, and 12, expressed *CD14* and *CD68* (**Figure 1B**, **C**) and isolating and reclustering of these cells revealed five distinct phenotypes (My.0-My.4, **Figure 4A**, **Online Figure 6A**, **Online Table 2**).

My.0, My.1 and My.2 most likely represented different macrophage activation states. Enrichment of pro-inflammatory marker genes (**Figure 4B**) and immune- and inflammatory pathways (**Figure 4C**) indicated that subclasses My.0 and My.1 consisted of pro-inflammatory macrophages. My.0 showed characteristics of recently recruited macrophages (''Leukocyte transendothelial migration'', Figure 4C and ''Leukocyte extravasation signaling'', **Figure 4D**) displaying inflammasome activation based on co-expression of *IL1B*, *CASP1* and *CASP4* (**Figure 4B**, **Online Figure 6B**). My.1 represented macrophages that differentially expressed *TNF* and toll-like receptors (**Figure 4B**). Interestingly, both My.0 and My.1 expressed *KLF4*, albeit at a low level, which is known to drive macrophages towards an anti-inflammatory phenotype by repressing the NF-κB gene program.[41] Our data may suggest that an inhibitory feedback loop in the pro-inflammatory macrophage populations is actively mediated by KLF4 expression.

In contrast to My.0 and My.1, My.2 showed absence of clear pro-inflammatory markers and showed signs of macrophages and foam cells. It expressed foam cell marker genes *ABCA1*[42], *ABCG1*, *MMP9*, and *OLR1*[43] (**Figure 4B**, **Online Figure 6A**), pro-fibrotic markers such as *TREM2* and *CD9*[44,45], and the enrichment of metabolic pathways hinted at a shift in metabolism (**Figure 4C** bottom). Interestingly, My.2 cells expressed smooth muscle actin (*ACTA2*), a hallmark of smooth muscle cells, in combination with macrophage markers such as *LGALS3* and *CD68* (**Online Figure 6C**, **D**). Expression of myeloid lineage transcription factors (TFs) PU.1 (SPI1) and C/EBPβ (CEBPB)[46] and absence of SMC lineage TFs myocardin (MYOCD) and MRTF-A (MRTFA)[47] in specifically the ACTA2^{+} cells of My.2 suggests that part of the My.2 myeloid cells gained characteristics of SMCs rather than that it originated from SMCs[17] (**Online Figure 6E**).

To further characterize the 3 subclasses, we next examined pathways differentially enriched per population (**Figure 4D**) as well as the upstream regulators that possibly govern these populations by Ingenuity Pathway Analysis (IPA; **Figure 4E**). My.0 and My.1 showed enrichment for classical inflammatory and immune pathways clearly suggesting cellular activation, recruitment and immune cell interactions driving their phenotype. In line, IPA predicted that My.0 and My.1 are mainly controlled by pro-inflammatory factors such as IL1A, IFNA, INFG and IL1B.

My.2 was enriched for metabolic pathways and LXR/RXR activation, consistent with a foamy phenotype. Hence, this cluster was uniquely driven by anti-inflammatory pathways such as STAT6 and had typical foam cell-related factors including APOE and the LXR family (Nr1h: NR1H2,3,4), which interestingly showed some overlap with My.1. The latter may indicate that unlike the more recently recruited My.0, My.1 cells are gaining foamy characteristics.

My.3 is characterized by dendritic cell (DC) markers such as *CD1C*, *CLEC10A*, and *FCER1A* **Online Figure 6A**) and this population most likely represents CD1c^{+} DCs.[13,48,49] In line with their DC phenotype, this cluster showed the highest expression of multiple class II HLA genes indicative of their enhanced activation status as a consequence of antigen-specific interaction with plaque T cells (**Online Figure 6F**). Cluster My.4 expressed *CD3E*, *GNLY*, *FOXP3*, and *CD2,* suggesting that My.4 potentially contains regulatory T cells. This mis-clustering might be a result of comparable CD4 expression levels in T cells and macrophages, since myeloid cells frequently expressed CD4 (**Online Figure 1E**).

Finally, we compared our macrophage subclasses with monocyte and macrophage populations from four recent papers on scRNA-seq analysis of atherosclerotic plaques in mice.[3–6] Eight mouse populations showed significant overlap with our human subclasses (**Figure 4F**). My.0 showed no statistically significant overlap, but most resembled inflammatory mouse macrophages (**Figure 4G**). My.1 resembled inflammatory, resident-like mouse macrophages, and My.2 overlapped with foamy, anti-inflammatory, Trem2^{+} macrophages. Together, this confirms the recently migrated and embedded inflammatory phenotypes we defined respectively for My.0 and My.1, and matches the foamy phenotype we saw in My.2. It also showcases a decent concordance between human patients and mouse models in relation to cell type diversity.

Intercellular communication drives inflammation within the plaque

We next examined potential ligand-receptor interactions between cell types to predict intercellular communication within the lesion based on CellPhone DB v2.0[50]. Lymphocytes and mast cells showed the lowest absolute numbers of potential interactions while myeloid, endothelial, and SMCs displayed higher numbers of interactions (**Figure 5A**). The low interaction between myeloid and T cells may be a consequence of the apparent lack of detection of TCR-related genes (*TRA, TRB, TRG)* in our scRNAseq dataset and the fact that CD4-class II and CD8-class I interactions are not included in this database.

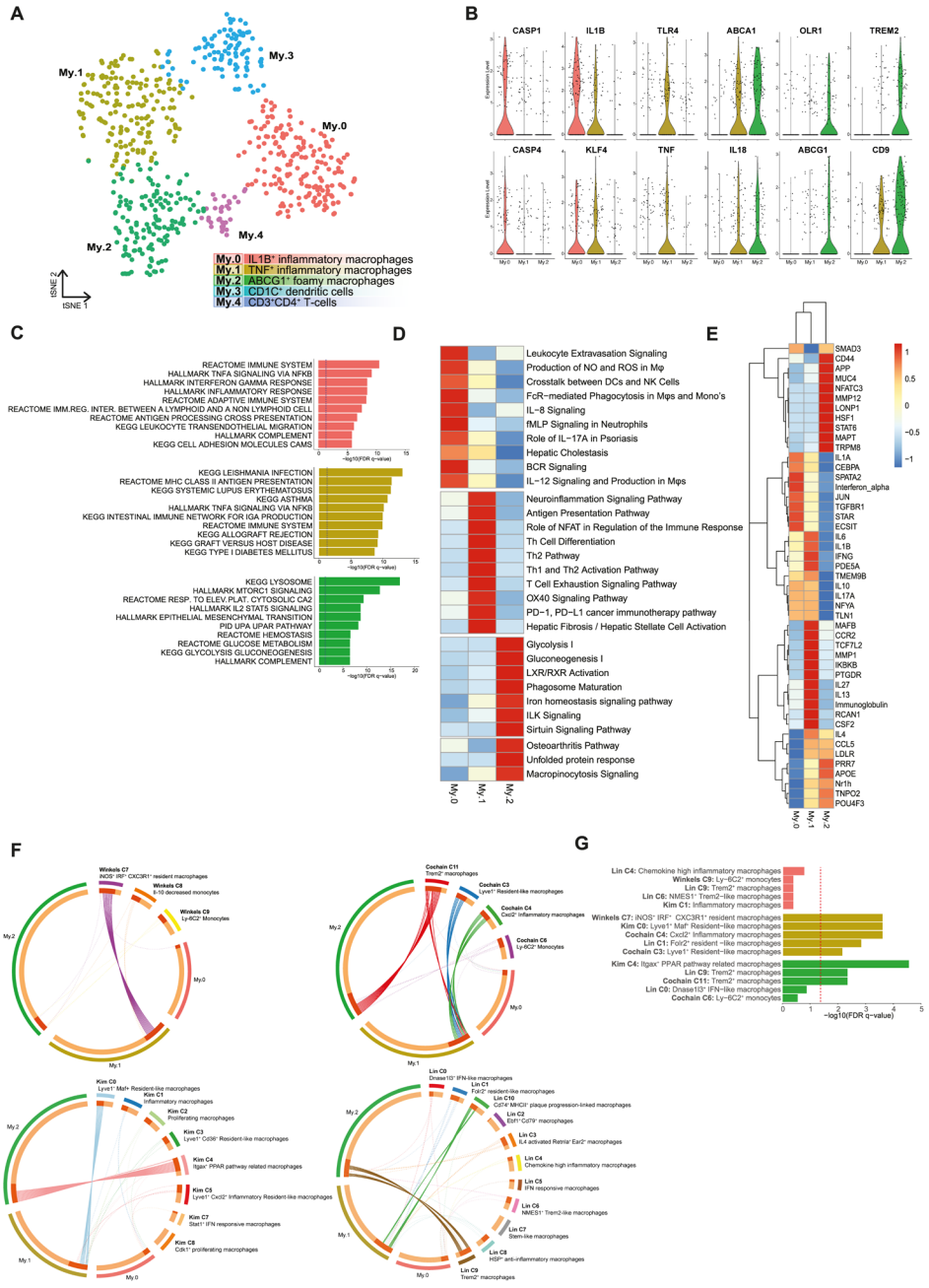
A
My.1
My.3
My.0
My.2
My.4
My.0 IL1B+ inflammatory macrophages
My.1 TNF+ inflammatory macrophages
My.2 ABCG1+ foamy macrophages
My.3 CD1C+ dendritic cells
My.4 CD3+CD4+ T-cells
tSNE 2
tSNE 1
B
CASP1
IL1B
TLR4
ABCA1
OLR1
TREM2
CASP4
KLF4
TNF
IL18
ABCG1
CD9
C
REACTOME IMMUNE SYSTEM
HALLMARK TNFA SIGNALING VIA NFKB
HALLMARK INTERFERON GAMMA RESPONSE
HALLMARK INFLAMMATORY RESPONSE
REACTOME ADAPTIVE IMMUNE SYSTEM
REACTOME IMM.REG. INTER. BETWEEN A LYMPHOID AND A NON LYMPHOID CELL
REACTOME ANTIGEN PROCESSING CROSS PRESENTATION
KEGG LEUKOCYTE TRANSENDOTHELIAL MIGRATION
HALLMARK COMPLEMENT
KEGG CELL ADHESION MOLECULES CAMS
KEGG LEISHMANIA INFECTION
REACTOME MHC CLASS II ANTIGEN PRESENTATION
KEGG SYSTEMIC LUPUS ERYTHEMATOSUS
KEGG ASTHMA
HALLMARK TNFA SIGNALING VIA NFKB
KEGG INTESTINAL IMMUNE NETWORK FOR IGA PRODUCTION
REACTOME IMMUNE SYSTEM
KEGG ALLOGRAFT REJECTION
KEGG GRAFT VERSUS HOST DISEASE
KEGG TYPE I DIABETES MELLITUS
KEGG LYSOSOME
HALLMARK MTORC1 SIGNALING
REACTOME RESP. TO ELEV.PLAT. CYTOSOLIC CA2
HALLMARK IL2 STAT5 SIGNALING
HALLMARK EPITHELIAL MESENCHYMAL TRANSITION
PID UPA UPAR PATHWAY
REACTOME HEMOSTASIS
REACTOME GLUCOSE METABOLISM
KEGG GLYCOLYSIS GLUCONEOGENESIS
HALLMARK COMPLEMENT
−log10(FDR q−value)
D
Leukocyte Extravasation Signaling
Production of NO and ROS in Mφ
Crosstalk between DCs and NK Cells
FcR−mediated Phagocytosis in Mφs and Mono's
IL−8 Signaling
fMLP Signaling in Neutrophils
Role of IL−17A in Psoriasis
Hepatic Cholestasis
BCR Signaling
IL−12 Signaling and Production in Mφs
Neuroinflammation Signaling Pathway
Antigen Presentation Pathway
Role of NFAT in Regulation of the Immune Response
Th Cell Differentiation
Th2 Pathway
Th1 and Th2 Activation Pathway
T Cell Exhaustion Signaling Pathway
OX40 Signaling Pathway
PD−1, PD−L1 cancer immunotherapy pathway
Hepatic Fibrosis / Hepatic Stellate Cell Activation
Glycolysis I
Gluconeogenesis I
LXR/RXR Activation
Phagosome Maturation
Iron homeostasis signaling pathway
ILK Signaling
Sirtuin Signaling Pathway
Osteoarthritis Pathway
Unfolded protein response
Macropinocytosis Signaling
My.0
My.1
My.2
E
SMAD3
CD44
APP
MUC4
NFATC3
MMP12
LONP1
HSF1
STAT6
MAPT
TRPM8
IL1A
CEBPA
SPATA2
Interferon_alpha
JUN
TGFBR1
STAR
ECSIT
IL6
IL1B
IFNG
PDE5A
TMEM9B
IL10
IL17A
NFYA
TLN1
MAFB
CCR2
TCF7L2
MMP1
IKBKB
PTGDR
IL27
IL13
Immunoglobulin
RCAN1
CSF2
IL4
CCL5
LDLR
PRR7
APOE
Nr1h
TNPO2
POU4F3
F
Winkels C7: iNOS+ IRF+ CXC3R1+ resident macrophages
Winkels C8: IL-10 decreased monocytes
Winkels C9: Ly-6C2+ Monocytes
Cochain C11: Trem2+ macrophages
Cochain C3: Lyve1+ Resident-like macrophages
Cochain C4: Cxcl2+ Inflammatory macrophages
Cochain C8: Ly-6C2+ Monocytes
Kim C0: Lyve1+ Maf+ Resident-like macrophages
Kim C1: Inflammatory macrophages
Kim C2: Proliferating macrophages
Kim C3: Lyve1+ Cd36+ Resident-like macrophages
Kim C4: Itgax+ PPAR pathway related macrophages
Kim C5: Lyve1+ Cxcl2+ Inflammatory Resident-like macrophages
Kim C7: Stat1+ IFN responsive macrophages
Kim C8: Cdk1+ proliferating macrophages
Lin C0: Dnase1l3+ IFN-like macrophages
Lin C1: Fcls2+ resident-like macrophages
Lin C10: Cd14+ MHCII+ plaque progression-linked macrophages
Lin C2: Ednrb+ Cd79+ macrophages
Lin C3: IL4 activated Retnla+ Ear2+ macrophages
Lin C4: Chemokine high inflammatory macrophages
Lin C5: IFN responsive macrophages
Lin C6: NME51+ Trem2-like macrophages
Lin C7: Stem-like macrophages
Lin C8: HSP+ anti-inflammatory macrophages
Lin C9: Trem2+ macrophages
My.0
My.1
My.2
G
Lin C4: Chemokine high inflammatory macrophages
Winkels C8: Ly−6C2+ monocytes
Lin C9: Trem2+ macrophages
Lin C6: NME51+ Trem2−like macrophages
Kim C1: Inflammatory macrophages
Winkels C7: iNOS+ IRF+ CXC3R1+ resident macrophages
Kim C0: Lyve1+ Maf+ Resident−like macrophages
Cochain C4: Cxcl2+ Inflammatory macrophages
Lin C1: Fcrl2+ resident −like macrophages
Cochain C3: Lyve1+ Resident−like macrophages
Kim C4: Itgax+ PPAR pathway related macrophages
Lin C9: Trem2+ macrophages
Cochain C11: Trem2+ macrophages
Lin C0: Dnase1l3+ IFN−like macrophages
Cochain C6: Ly−6C2+ monocytes
−log10(FDR q−value)

◂ **Figure 4. Subclustering of myeloid cells revealed 5 distinct populations.** A) tSNE visualization of clustering revealed 5 distinct myeloid populations. B) Violin plots of macrophage-specific activation genes and foam cell markers. C) Top pathways associated with the macrophage clusters. D) Unique pathways per macrophage cluster. E) IPA analysis of upstream regulators of the macrophage subsets. Both D and E depict data as Z-score. F) Circos plots displaying overlap of macrophage clusters with macrophage clusters of murine scRNA-seq papers. Dotted lines indicate no significant overlap, solid lines indicate significant overlap. G) Bar graph with top 5 overlapping clusters of human and murine macrophage clusters.

Subsequently, we specifically examined the top unique interactions within the myeloid populations, split by myeloid ligands (**Figure 5B**) and receptors (**Figure 5C**). We found multiple chemotactic interactions, including endothelial *ACKR1*[51] with myeloid derived *CCL2*, CXCL8, *CCL8* and *CXCL1*, of which the last two ligands were specifically expressed in My.1. We also observed an interaction between *CSF1R* on all myeloid subsets and *CSF1* on endothelial cells, smooth muscle cells, mast cells and myeloid cells. *CCR1* and *CCR5* interacted with CCL5 from both $CD4^+$ and $CD8^+$ T cells and *CXCR4* on B cells interacted with *CXCL12* on My.1 cells. In addition, we identified communication patterns that are potentially involved in extravasation of myeloid cells, including *CD44* (My) – *SELE* (EC), *SELL* (My) – *CD34* (EC), *SELPLG* (My) – *SELP* and *SELL* (both EC). Myeloid cells showed potential capability to attract other leukocytes, for example $CCR5^+$ T cells through expression of *CCL3* (My.1). Moreover, myeloid cells were also predicted to interact with T cells leading to mutual activation, through i.e. *SIRPA* (My) – *CD47* (T)[52], *ICAM1* (My) – *ITGAL* (CD8), inducing cytotoxicity, and multiple interactions involved in antigen presentation. Lastly, interaction of *PDGFB* on myeloid subsets with *PDGFBR* on endothelial cells suggest a possible myeloid-driven induction of angiogenesis, which has been associated with plaque destabilization.[53,54]

Chromatin accessibility of myeloid and T cell populations reveals transcription factors involved in gene regulation

Next, we aimed to further define the genomic landscape that accounts for the obtained cluster-specific patterns of gene expression and potentially uncover disease driving transcription factors. Using scATAC-seq we examined the open chromatin promoter and enhancer landscape of myeloid- and T cells in human plaques. We identified four myeloid and five T cell clusters by scATAC-seq. Population label transfer from scRNA-seq to scATAC-seq populations showed good agreement with the native scATAC-seq cluster borders and retrieved the majority of the scRNA-seq populations (**Figure 6A**, **B**). Open chromatin at macrophage (*CSF1R*, *IL1B*) and T cell specific genes (*NKG7*), as well as enrichment of motifs of cell-type TFs for macrophages and T cells (*SPI1*[55] and *ETS1*[56]), confirmed the delineation between cell types (**Figure 6C**, **D**). Transferred myeloid populations were reclustered analogous to the scRNA-seq clusters (**Figure 6E**).

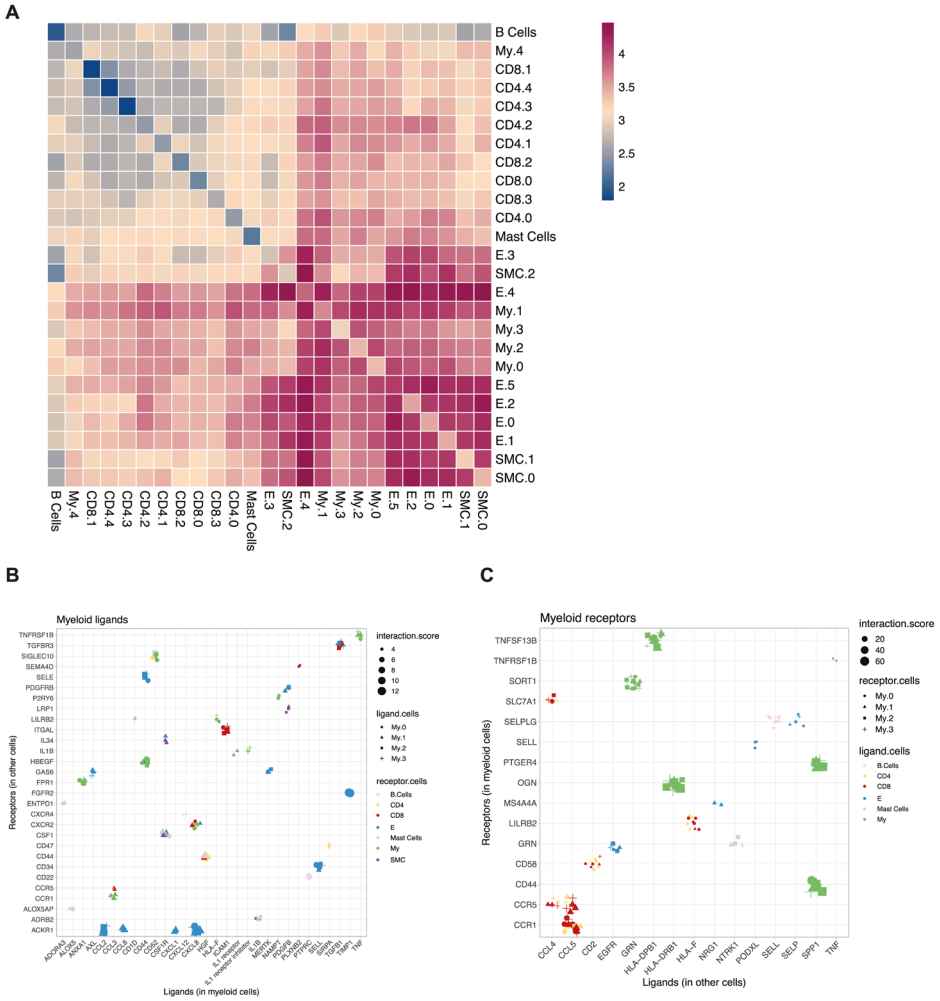

Figure 5. Ligand-receptor interaction analyses to asses intracellular communication in the plaque. A) Heatmap showing logarithmic interaction scores between all cell subsets. Top quartile of unique ligand-receptor interactions between all cells and myeloid cells for both B) ligands expressed by myeloid cells and C) receptors expressed by myeloid cells.

IRF4 has been shown to be a CD1c^{+} dendritic cell-specific transcriptional regulator[57] and its motif was indeed enriched in My.3 (**Figure 6F**). In line, we found specific open chromatin at the promoter region of *IL12A*, the subunit that is specific for the cytokine IL12, in all myeloid populations and an enhancer specifically in My.3 dendritic cells (**Online Figure 7E**). IL12 is required to induce a pro-inflammatory, T_H1-like cytotoxic phenotype of T cells and actively induces atherosclerosis.[58,59] Potentially, as a result of the My.3-specific IL12, we observed open chromatin at the *IFNG* and *TNF* loci in

CD4.0, confirming its activated, cytotoxic phenotype and suggesting that this cluster has T_H1-like properties. (**Online Figure 7G**, **H**). Additionally enriched accessible motifs within the T cells (**Online Figure 7A**, **B**) were observed for the *RUNX3* motif in CD4.0, normally a $CD8^+$ T cell linage specific TF that is also known to induce expression of cytotoxic genes in $CD4^+$ T cells[60–63], as well as the *STAT3* motif, which is downstream of IL6 and IL2 signaling. The BATF_JUN motif (**Online Figure 7C**) that is known to be critical for effector function in T cells, was also enriched in this cluster.[64] The effector function could be further confirmed by differential open chromatin of the *GZMB* and *GZMH* loci in both CD4.0 and all CD8 clusters (**Online Figure 7D**) and an open locus at *IL2* in CD4.0, CD4.1 and CD8.0.

In line with the scRNA-seq data My.1 showed enrichment of pro-inflammatory TF motifs (**Figure 6F**), which matches the pro-inflammatory gene expression seen in these cells. This cluster was especially enriched in interferon signaling induced TFs including IRF1, IRF9, STAT1 and STAT2. The STAT1-STAT2 complex is known to interact with IRF9 upon IFNγ stimulation and hence induces the upregulation of pro-inflammatory cytokines as TNF, indicating an IFNγ pathway driven activation, possibly secreted by the T cells.[65] Indeed, the IRF9 motif was accessible and the *IRF9* locus was open predominantly in My.1 cells (**Figure 6G**, **H**). Moreover, these IRF and STAT TFs are also key mediators of type I IFN responses which have previously been shown to associate with atherosclerotic disease as well.[66]

My.0 cells were specifically enriched for the NFATC3 motif (**Figure 6F**), a TF which has previously been linked to activated TLR-pathway signaling and has been shown to partially regulate subsequent TNFα and IL-1β secretion.[67,68] Finally, My.2 cells were enriched for anti-inflammatory, foam cell associated TFs in the scATAC-seq data similar as in the scRNA-seq data. We observed increased chromatin accessibility at loci harboring the KLF4 motif, which next to repressing pro-inflammatory programs was shown to implement an anti-inflammatory macrophage activation state and is also known to be involved in the transformation of vascular SMCs to macrophages[41,46,69] (**Figure 6F**). This is in contrast with the scRNA-seq data where KLF4 was expressed at a low level, indicating that while the KLF4 locus is poised, its associated gene program is not necessarily executed in all foamy macrophages. Furthermore, My.2 was enriched for the *de novo* motif MA1149.1, which was annotated to RAR_RXR, a motif with high similarity to the LXR_RXR motif (**Figure 6I**). Moreover, LXR_RXR motif accessibility is enriched in My.2 cells and the *NR1H3* (LXRα) locus is opened specifically in the My.2 population (**Figure 6J**). In line, the scRNA-seq data likewise shows *NR1H3* upregulation specifically in My.2 (**Figure 6K**).

We could not map the regulatory T cell cluster CD4.3 to an scATAC-seq cluster. The *FOXP3* locus hardly showed open chromatin in any population in the scATAC-seq data set and neither did the Treg-associated cytokine gene *IL10* (**Online Figure 7I**, **J**).

Cell type specific enrichment of genes in GWAS loci

Genome wide association studies (GWAS) have discovered 163 genetic susceptibility loci linked to coronary artery disease (CAD) through literature search and effects on expression[70]. However, the challenge remains in identifying the potential causal genes linked to these loci for functional testing as novel therapeutic targets. In part, this is due to the underlying genetic architecture where multiple causative variants in a gene might be involved and variants in linkage disequilibrium only show marginal significance in a GWAS. Another reason is that many of the risk variants are not causal and ambiguously linked to genes. A gene-centric analysis considers all variants in a gene and solves these issues, yet such analyses fail to identify the cells potentially involved. Here, we aimed to 1) identify genes associated to CAD, that are 2) also highly expressed in specific cell types, effectively identifying tangible candidates for functional follow-up. To this end, we mapped genes near GWAS loci associated to CAD, and assessed expression of these genes across our scRNA-seq cell populations to investigate their expression in disease relevant tissue. We prioritized 317 protein-coding genes based on the summary statistics of a recent CAD GWAS[71] (see **Online Methods**; **Online Table 3**). Next, we selected the genes that would best represent each individual cell population. To achieve this, we determined differentially expressed genes (DEGs) (**Online Figure 8**; Online Methods). 3876 genes were differentially expressed and DEGs were grouped into 15 gene expression patterns that best matched the scRNA-seq populations (**Figure 7A**). We overlapped the 317 CAD associated genes with the 3876 differentially expressed genes, resulting in a significant overlap (permutation over random data $p = 2{,}67e^{-5}$) of 74 genes. These genes are distributed over multiple individual CAD loci (**Online Table 3**), indicating that our methods are robust. We observed a significant accumulation of GWAS linked genes in patterns 3, 8 and 14 (permutation over random data p = 0.015, p = 0.006 and p = 0.015 respectively) (**Figure 7B**). Genes in pattern 3 are associated with higher expression in the endothelial cell clusters 9 and 10 (**Figure 7C**) and consisted of *SHE*, *KCNN3*, *VAMP5*, *SEMA3F*, *HDAC9*, *GIMAP1*, *NOS3*, and *DOCK6*. Pattern 8 is hallmarked by gene expression associated with all four macrophage populations (**Figure 7A**) and contained *AMPD2*, *CTSS*, *IL6R*, *CAPG*, *GPX1*, *GNAI2*, *TRIB1*, *SH2B3*, *FES*, *C19orf38* and *VASP* (**Figure 7B**, **D**). Genes in pattern 14 were predominantly associated with higher expression in both the smooth muscle cell population 8 and the *CD34*$^{+}$ endothelial cell population 10 (**Figure 7E**). This pattern contained *ITGB*, *ARHGEF26*, *CXCL12*, *PTPN11*, *COL4A1*, *COL4A2*, *KANK2* and *GGT5*. Our results suggest that macrophages, smooth muscle cells and endothelial cells are of particular interest as a starting point for functional testing.

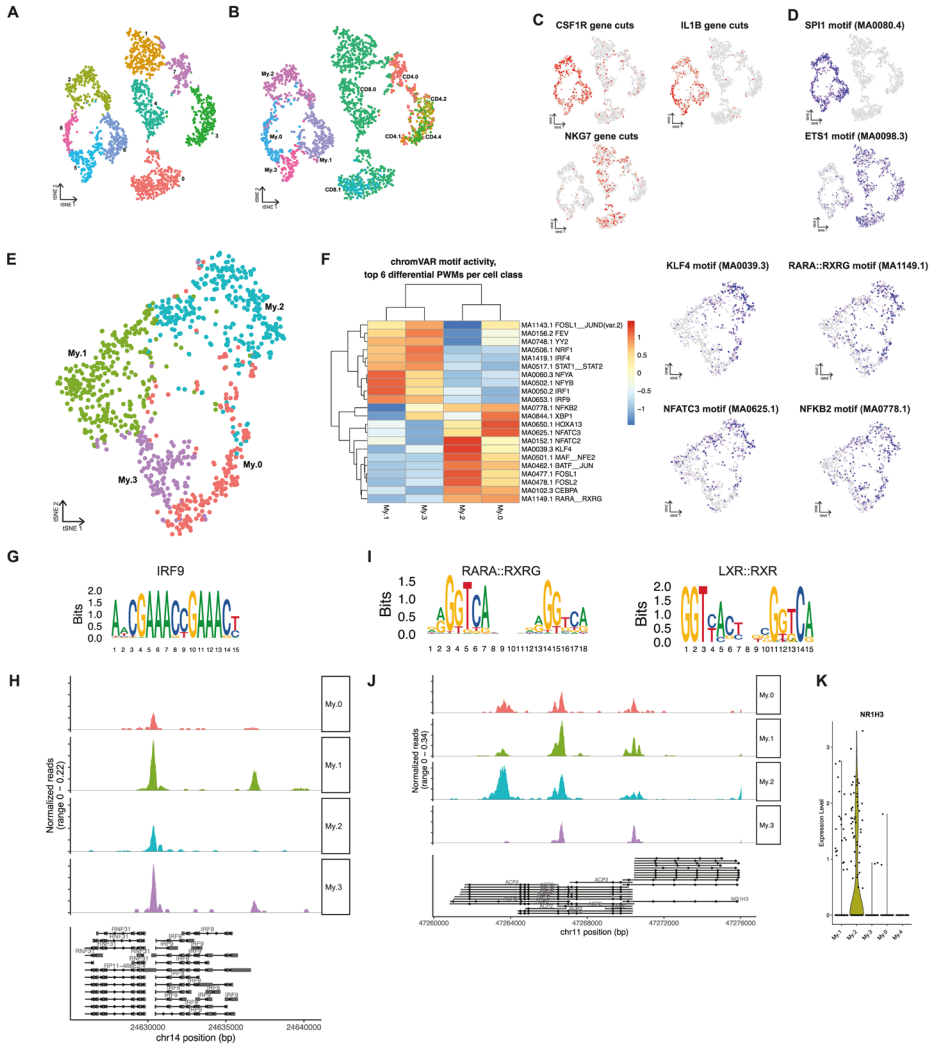

Figure 6. Chromatin accesibility of myeloid cells in human atherosclerotic plaques analyzed using scATAC-seq. A) tSNE visualization of myeloid and T cell clusters based on scATAC-seq. B) Projection of scRNA-seq myeloid and T cell labels over the scATAC-seq clusters. C) tSNE visualization of cell type-specific accessible gene loci. D) tSNE visualization of cell type-specific transcription factor motifs enriched in open chromatin regions. E) tSNE visualization of subclustered scATAC-seq myeloid clusters. F) Heatmap showing the top differential open chromatin TF motifs by chromVAR, with subcluster specific accessible TF motifs visualized as tSNE. G) IRF9 motif H) Pseudobulk genome browser visualization identifying the open chromatin regions of *IRF9* in different myeloidsubsets. I) RARA:RXRG and LXR:RXR motifs. J) Pseudobulk genome browser visualization identifying open chromatin regions of *NR1H3* (encoding LXRα) in different myeloid subsets. K) Violin plot of *NR1H3* gene expression from myeloid scRNA-seq data.

Furthermore, given that for many of the genes previously mapped to the 163 CAD loci the mechanisms and cellular expression are still unknown[70], we examine whether these genes show cell-type specific expression in carotid plaques. We found that 24 of the 75 genes previously classified as 'unknown' by Erdmann *et al*.[70] were differentially expressed between cell populations in carotid plaques, and included 3 genes that also showed association with CAD (*CHD13*, *SNRPD2* and *ARHGEF26*; **Online Table 3**) in our analysis.

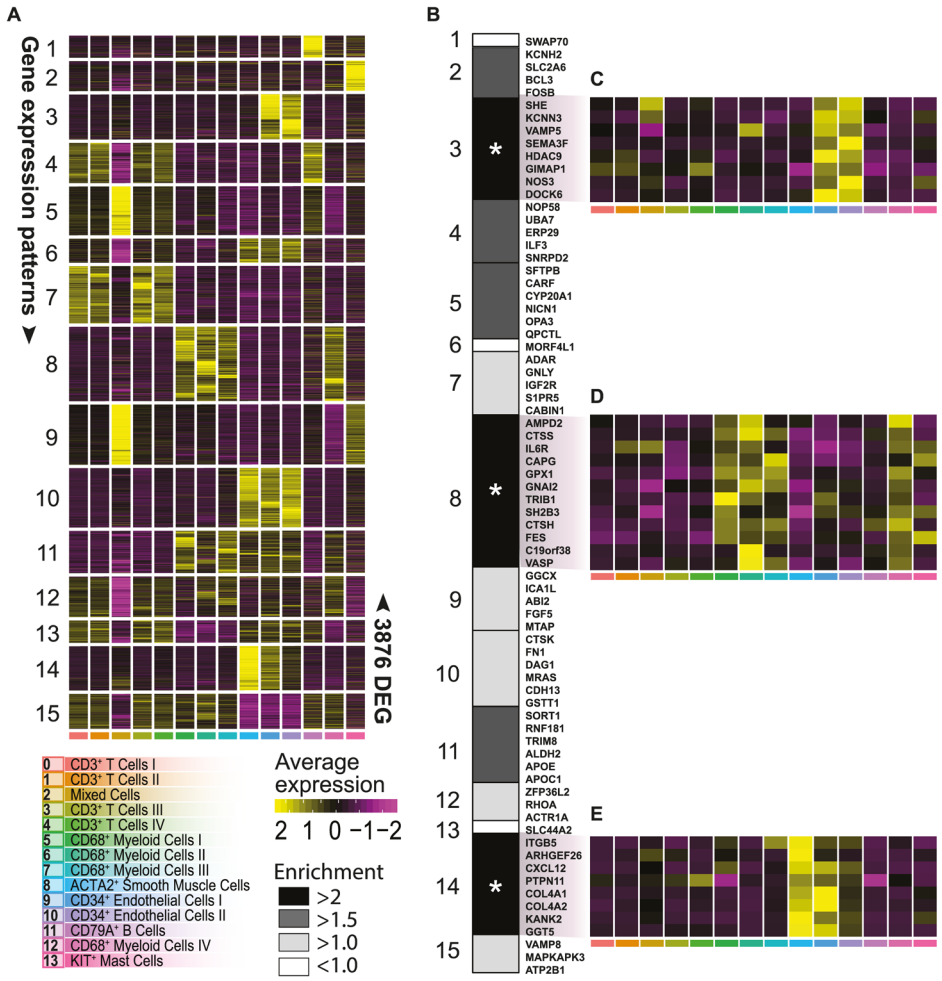

Figure 7. Projection of CAD GWAS associated genes. A) Heatmap of average expression of 3876 DEGs divided into 15 gene expression patters that best matched cluster or cell-type identity (for DEG selection, see **Online Figure 8**). B) Enrichment of 74 CAD GWAS associated genes across the 15 gene expression patterns. C, D, E) Heatmap of average relative expression of significantly enriched CAD genes from gene expression pattern #3, #8 and #14 respectively. Asterisk indicates significant enrichment. *p<0.05.

Discussion

In the past two years, single-cell technologies have advanced our knowledge in atherosclerosis tremendously. scRNA-seq has been applied to specifically describe the immune cell landscape of murine and human atherosclerotic lesions.[3–7] The recent study by Fernandez *et al*. gave a first overview of the human immune cell landscape during atherosclerosis by showing a data set based on extensive CyTOF analyses and by comparing RNA expression profiles of T cells and macrophages in plaque and blood of symptomatic and asymptomatic patients[7]. They provide insight into which immune cells reside in the plaque and described their different activation states. Yet, both the mouse and human studies lack coverage of non-immune cell types in the plaque and so far only a limited number of patients have been included in the scRNA-seq studies. Here, we applied scRNA-seq to all live cells in advanced human atherosclerotic plaques of 18 patients and revealed a highly diverse cellular landscape consisting of 14 main cell populations.

We detected a predominance of T cells in the leukocyte population of the human lesions. In contrast, murine scRNA-seq studies describe a more prominent presence of myeloid cells, which may be caused by the previously described declining myeloid content upon progression of human atherosclerotic plaques, whereas T cells reciprocally increase in human atherosclerosis.[72,73] Both $CD4^+$ and $CD8^+$ T cells subsets were characterized by their activation state, rather than classical T_H or T_C subclasses. We could confirm the presence of activated T cells that in the plaque could especially be characterized by the expression of multiple granzymes.[7] In addition, we show that these granzymes are not only expressed by $CD8^+$ T cells, but also by a substantial number of $CD4^+$ T cells in the plaque. The $CD4^+$ T cells showed a dominant cytotoxic T cell pool, characterized by expression of *PRF1* and multiple granzymes, with granzyme B production confirmed by flow cytometry. The lack of *CD28* expression in these cells indicates that this pool constitutes most likely a subset of cytotoxic $CD4^+CD28^{null}$ T cells, which has previously been associated with atherosclerosis as they have been detected in peripheral blood of CAD patients.[30,74] Although the presence of a similar TCR clone as observed in peripheral $CD4^+CD28^{null}$ cells was found in bulk coronary artery tissue[30,74], we can now confirm the presence of these cells on a single-cell level suggesting a functional role in patients with CVD. As cytokine expression could not be retrieved from the scRNA-seq data, but we were able to detect open chromatin at various cytokine gene loci within the T cell populations using scATAC-seq suggesting active cytokine genes. Amongst others, *IFNG* showed open chromatin in the cytotoxic and effector T cell subclasses. Apart from confirming the cytotoxic, T_H1-like phenotype within the plaque, this also suggests that the pro-inflammatory

macrophage subclasses we observe in our dataset may be primed for classical activation by secretion of IFNγ by the T cells.[75] These T_H1 cells acting on macrophages may in turn be driven by activated CD1c$^+$ dendritic cells that were characterized by an active *IL12* gene (i.e. open enhancer), which has previously been found on protein level in plaque lysates[76,77], and the enrichment of HLA-DR subtypes.[78,79]

Each of the macrophage clusters seemed to have been activated differently, one expressing *TNF* and *TLR4*, which can be activated by oxLDL and IFNγ[80], as well as IL1B, and the other more selectively expressing *IL1B*, which correlated with caspase expression suggesting inflammasome activation.[81] The recent CANTOS trial, which targeted IL-1β[82], might thus have been effective through impacting on the pro-inflammatory capacity of the My.0 and My.1 populations within the plaque. Chromatin accessibility confirmed the pro-inflammatory phenotype of these cells by showing open regions linked to inflammatory transcription factors. Particularly the TNF enriched macrophage cluster My.1 was enriched for motifs from IFN induced TFs (e.g. STATs, IRFs), which correlated with our upstream regulator analysis that suggested IFN as drivers of the macrophage phenotype and may be a result of the local IFNγ production by T cells. In line, the My.0 and My.1 populations correlated with inflammatory and resident-like macrophages as detected in murine lesions. [3–6]

The IL12–IFNγ-axis, as found in our scRNA-seq, data may form an important feature of T cell activation in the plaque, and subsequent activation of myeloid cells contributes to the inflammation profile within the plaque. This is in line with several experimental studies that show the pro-atherogenic role of both IL12 and IFNγ in cardiovascular disease.[59,83,84]

The more anti-inflammatory foam-cell-like cluster was characterized by expression of ABC cholesterol efflux transporters and lipid-related genes whose expression is most likely driven by intracellular lipid accumulation.[85] The lipid-phenotype was confirmed by the enriched LXR_RXR TF motifs in the scATAC-seq data. LXR is a well-known nuclear receptor, active in foam cells and inducing ABC transporters.[46,86] The notice that foam cell formation per se is not pro-inflammatory is a recent ongoing paradigm shift in the field. Several studies have previously shown clear pro-inflammatory characteristics of foam cell formation, either through engagement of TLRs by oxLDL[87–89], induction of oxidative responses[90] or through other pathways.[91–93] However, recent data studying foam cells in in vivo model systems[94] or isolating foam cells from murine plaques[5] clearly demonstrate that foam cells do not necessarily show pro-inflammatory characteristics and even may be considered anti-inflammatory.[94,95] In line, our data shows that cells exhibiting the foam-cell driven LXR activation program do not express

high levels of *IL1B* and *TNF*. This further confirms that lipid accumulation leads to *LXR* activation and induces an anti-inflammatory phenotype. We also observed *TREM2* and *CD9* expression within this cluster, resembling the TREM2$^+$ macrophages found in murine atherosclerosis.[4,6] In other tissues, these TREM2$^+$CD9$^+$ macrophages have been described as either Lipid Associated Macrophages (LAMs)[45] in obesity, or as Scar Associated Macrophages (SAMs)[44] in liver cirrhosis. Key phenotypes of these cells were shown to involve pro-fibrotic characteristics and this is also of high relevance for human atherosclerosis as it may indicate a plaque stabilizing macrophage population.

Our study provides further supports the notion that trans-differentiation of cells is likely to occur in human atherosclerosis. About a quarter of the My.2 macrophages expressed smooth muscle cell actin, which may indicate derivation from SMCs, or conversely macrophages showing a SMC cell-like fibrotic phenotype.[17,96] Presence of myeloid lineage specific TF expression in these cells (e.g. SPI and CEBPB) and absence of SMC TFs (e.g. MYOCD and MRTFA) suggests that the latter is more likely. This is in line with previous reports applying SMC lineage tracing that showed that unidentified SMC-derived cells in atherosclerotic lesions exhibit phenotypes of other cell lineages, including macrophages and mesenchymal stem cells.[17,97] Also endothelial cell cluster E.3 was characterized by expression of smooth muscle cell markers, such as *ACTA2*, *MYH11* and *NOTCH3*, suggesting that these cells could be in endothelial to mesenchymal transition. Mature endothelial cells can exhibit considerable heterogeneity and can transdifferentiate into mesenchymal-like cells, a biological process called EndoMT.[97] There is accumulating evidence that EndoMT plays a role in atherosclerotic lesion progression and which has been linked with inflammatory stress and endothelial dysfunction.[98,99] Our study shows that distinct EC clusters are present within atherosclerotic lesions and the gene signatures identify a cluster that shares both SMC and EC characteristics further providing human supportive evidence that EndoMT may occur in advanced human atherosclerotic plaques.

Apart from cellular plasticity within the endothelial and macrophage population, our study also provides new insights regarding intercellular communication within the plaque and its role in progression of atherosclerosis. We have shown that the within the plaque this was predicted to be most prevalent between myeloid, endothelial and smooth muscle cells. In addition to previous studies predicting interactions between macrophages and T cells in human lesions[7], we were also able to predict interactions between endothelial cells and SMCs, which were mainly involved with chemotaxis and extravasation of myeloid cells. We also show activation and recruitment of other immune cells, in particular T cells. Future development of therapeutics may benefit from detailing these interactions, providing specific pathways to target.

One of the significant post-GWAS challenges is the identification of candidate genes and pathways with clinical potential.[100] Here we mapped genes based on common variants (minor allele frequency > 1%) in susceptibility loci and used single-cell resolution expression in disease-relevant tissue to identify putative targets for future functional follow-up Our analysis showed enriched expression of CAD-associated genes in myeloid, endothelial, and smooth muscle cells. Furthermore, some of these genes are involved in cell-cell interactions, such as *SORT1* and *CXCL12*. Interestingly, the candidate genes did not show a significant overlap with T cells specific transcriptional signatures. Our approach is pragmatic in that we explicitly focus on 1) common variants in risk loci associated to CAD, and 2) map protein-coding genes that are associated to CAD to these risk loci, and 3) select CAD-associated genes that are also differentially expressed between cell populations. This identifies tangible potential targets as starting points for future functional testing in macrophages, endothelial and smooth muscle cells. However, we note that rare loss-of-function (LoF) variants and underrepresented genes may have significant effects in these and other cells. Future studies focusing on LoF variants and under-expressed genes could identify potentially other cell-specific targets.

There are several limitations that come with the use of human plaque endarterectomy samples. The vast majority of carotid endarterectomy samples also contain an inevitable small medial smooth muscle cell layer that potentially has contributed to the contractile smooth muscle cell cluster. There is a fine line between increasing digestion time to isolate more cells and generating a pure sample containing a high number of viable cells. We therefore not exclude that the ratio of cell types that we detected in the plaques based on gene expression profiles was affected by the digestion procedure.

In summary, we provide an in-depth characterization of the highly diverse cellular communities in advanced human atherosclerotic plaques. Based on RNA expression and chromatin accessibility profiles of individual cells, we uncover amongst others the presence of pro-inflammatory, cytotoxic T cell populations, multiple activation states of macrophages and their interactions, and functionally distinct endothelial cell populations that all can be considered modulators of human disease development. Furthermore, we show that by incorporating GWAS data, scRNA-seq data can be applied to map CVD susceptibility loci to specific cell populations and define potential patient-driven relevant targets for drug intervention of specific cell types. Our approach thus provides a powerful tool to aid research into the mechanisms underlying human disease and discover novel drug targets for intervention.

Funding

This work was supported by The Dutch Heart Foundation [CVON2017-20: Generating the best evidence-bases pharmaceutical targets and drugs for atherosclerosis (GENIUS II) to JK, MW, GP, SWvdL, MACD, IB, BS]; Spark-Holding BV [grant number 2015B002 to MW]; NWO-ZonMW [PTO program Inhibition of mast cell activation in atherosclerotic lesions using an anti-IgE antibody approach. [grant number 95105013, to MACD, IB, JK]; the European Union [ITN-grant EPIMAC to MW]; Fondation Leducq [Transatlantic Network Grants to MW, CKG, SY-H and GP]; EU 755320 Taxinomisis grant [GJdB, AB, GP]. We acknowledge the European Research Area Network on Cardiovascular diseases [ERA-CVD, grant number 01KL1802 to SWL, GP]; European Research Council (ERC) consolidator grant [grant number 866478 UCARE to HMdR]. MUK was supported by the ERC under the European Union's Horizon 2020 research and innovation programme [grant number 802825 to MUK], the Academy of Finland [Decisions 287478 and 319324], the Finnish Foundation for Cardiovascular Research and the Sigrid Jusélius Foundation. TÖ and MUK were supported by the Health from Science (TERVA) Programme of the Academy of Finland [Decision 314554]. TL was supported by the Academy of Finland [Decisions 311081 and 314557].

Acknowldegements

We would like to thank Judith Vivié and Dr. Mauro Muraro of Single Cell Discoveries for processing the plates for sequencing. We thank Dr. Anouk Wezel and Dr. Harm Smeets for sample collection at the Haaglanden Medisch Centrum. We acknowledge Biocenter Finland for infrastructure support. We are grateful to Kimmo Mäkinen for enabling sample acquisition at Kuopio University Hospital.

Author contributions

M.A.C.D., K.H.M.P. and L.S. drafted the manuscript and designed the figures. G.J.B. performed carotid endarterectomy procedures. M.A.C.D., D.E., I.B, B.S, S.C.A.J. and M.M. provided the pilot experiments. D.E. and M.A.C.D. executed the human plaque processing, FACS and flow cytometry. K.H.M.P. performed the clustering analyses. L.S. performed the GWAS analysis with help from M.M., S.W.L., A.B. and F.W.A. S.W.L. executed the FUMA data collection. M.A.C.D., K.H.M.P., L.S., A.B. I.B., B.S. and S.W.L. participated in conceptualization, data interpretation and provided critical feedback on the manuscript. S.C.A.J. and E.L. provided critical feedback on the manuscript. H.M.D.R. and C.K.G. provided funding and critical feedback on the manuscript. T.Ö., E.A. and T.L. processed the human plaque samples and carried out the experimental work for scATAC-seq, analyzed the data, and prepared the corresponding figures. M.U.K. and S.Y.-H. participated in the conceptualization,

funding and supervision of the scATAC-seq experiments and analysis. M.M., J.K., M.W. and G.P. participated in the conceptualization, funding and supervision of the scRNA-seq experiments and analysis and finalization of the manuscript. All authors provided feedback on the research, analyses and manuscript.

Disclosures

The authors have no conflicts of interest.

References

1. Benjamin, E. J. *et al.* Heart Disease and Stroke Statistics—2017 Update: A Report From the American Heart Association. *Circulation* **135**, e146–e603 (2017).
2. Turner, A. W., Wong, D., Dreisbach, C. N. & Miller, C. L. GWAS Reveal Targets in Vessel Wall Pathways to Treat Coronary Artery Disease. *Frontiers in Cardiovascular Medicine* **5**, 1–10 (2018).
3. Winkels, H. *et al.* Atlas of the Immune Cell Repertoire in Mouse Atherosclerosis Defined by Single-Cell RNA-Sequencing and Mass Cytometry. *Circ Res* **122**, 1675–1688 (2018).
4. Cochain, C. *et al.* Single-Cell RNA-Seq Reveals the Transcriptional Landscape and Heterogeneity of Aortic Macrophages in Murine Atherosclerosis. *Circ Res* **122**, 1661–1674 (2018).
5. Kim, K. *et al.* Transcriptome Analysis Reveals Nonfoamy Rather Than Foamy Plaque Macrophages Are Proinflammatory in Atherosclerotic Murine Models. *Circ Res* **123**, 1127–1142 (2018).
6. Lin, J.-D. *et al.* Single-cell analysis of fate-mapped macrophages reveals heterogeneity, including stem-like properties, during atherosclerosis progression and regression. *JCI Insight* **4**, (2019).
7. Fernandez, D. M. *et al.* Single-cell immune landscape of human atherosclerotic plaques. *Natuere Medicine* **25**, 1576–1588 (2019).
8. Aran, D. *et al.* Reference-based analysis of lung single-cell sequencing reveals a transitional profibrotic macrophage. *Nature Immunology* **20**, 163–172 (2019).
9. Müller, A. M. *et al.* Expression of the Endothelial Markers PECAM-1, vWf, and CD34 in Vivo and in Vitro. *Experimental and Molecular Pathology* **72**, 221–229 (2002).
10. Owens, G. K. Regulation of differentiation of vascular smooth muscle cells. *Physiological reviews* **75**, 487–517 (1995).
11. Germain, R. N. T-cell development and the CD4–CD8 lineage decision. *Nature Reviews Immunology* **2**, 309–322 (2002).
12. LeBien, T. W. & Tedder, T. F. B lymphocytes: how they develop and function. *Blood* **112**, 1570–80 (2008).
13. Ziegler-Heitbrock, L. *et al.* Nomenclature of monocytes and dendritic cells in blood. *Blood* **116**, e74-80 (2010).
14. Stöger, J. L. *et al.* Distribution of macrophage polarization markers in human atherosclerosis. *Atherosclerosis* **225**, 461–468 (2012).
15. Tabas, I. & Bornfeldt, K. E. Macrophage Phenotype and Function in Different Stages of Atherosclerosis. *Circulation research* **118**, 653–67 (2016).
16. Voehringer, D. Protective and pathological roles of mast cells and basophils. *Nature Reviews Immunology* **13**, 362–375 (2013).
17. Shankman, L. S. *et al.* KLF4-dependent phenotypic modulation of smooth muscle cells has a key role in atherosclerotic plaque pathogenesis. *Nat Med* **21**, 628–637 (2015).
18. Thiriot, A. *et al.* Differential DARC/ACKR1 expression distinguishes venular from non-venular endothelial cells in murine tissues. *BMC Biology* **15**, 1–19 (2017).
19. Kalucka, J. *et al.* Single-Cell Transcriptome Atlas of Murine Endothelial Cells. *Cell* **180**, 764-779. e20 (2020).
20. Adams, G. N. *et al.* Prolylcarboxypeptidase promotes angiogenesis and vascular repair. *Blood* **122**, 1522–1531 (2013).
21. Elices, M. J., Osborn, L., Luhowskyj, S., Hemler, M. E. & Lobb, R. R. VCAM-1 on activated endothelium interacts with the leukocyte integrin VLA-4 at a site distinct from the VLA-4.pdf. *Cell* **60**, 577–584 (1990).

22. Moreno, P. R., Purushothaman, K. R., Sirol, M., Levy, A. P. & Fuster, V. Neovascularization in human atherosclerosis. *Circulation* **113**, 2245–2252 (2006).
23. Zhu, L. *et al.* Mutations in myosin heavy chain 11 cause a syndrome associating thoracic aortic aneurysm / aortic dissection and patent ductus arteriosus. *Nature Genetics* **38**, 343–349 (2006).
24. Jin, S. *et al.* Notch Signaling Regulates Platelet-Derived Growth Factor Receptor-B Expression in Vascular Smooth Muscle Cells. *Circulation Research* **102**, 1483–1491 (2008).
25. Schlosser, A. *et al.* MFAP4 Promotes Vascular Smooth Muscle Migration ,. *Arterioscler Thromb Vasc Biol.* **36**, 122–133 (2016).
26. Rensen, S. S. M., Doevendans, P. A. F. M. & van Eys, G. J. J. M. Regulation and characteristics of vascular smooth muscle cell phenotypic diversity. *Neth Heart J* **15**, 100–8 (2007).
27. Luger, D. *et al.* Expression of the B-Cell Receptor Component CD79a on Immature Myeloid Cells Contributes to Their Tumor Promoting Effects. *PLoS ONE* **8**, e76115 (2013).
28. Tedder, T. F., Tuscano, J., Sato, S. & Kehrl, J. H. CD22 , A B LYMPHOCYTE – SPECIFIC ADHESION MOLECULE THAT REGULATES ANTIGEN RECEPTOR SIGNALING *. *Annu. Rev. Immunol* **15**, 481–504 (1997).
29. Liu, C., Richard, K., Melvin, W., Zhu, X. & Conrad, D. H. CD23 can negatively regulate B-cell receptor signaling. *Scientific reports* **6**, 1–8 (2016).
30. Liuzzo, G. *et al.* Monoclonal T-Cell Proliferation and Plaque Instability in Acute Coronary Syndromes. *Circulation* **102**, 2883–2888 (2000).
31. Liuzzo, G. *et al.* Unusual CD4+CD28null T Lymphocytes and Recurrence of Acute Coronary Events. *J Am Coll Cardiol* **50**, 1450–1458 (2007).
32. Mohr, A., Malhotra, R., Mayer, G., Gorochov, G. & Miyara, M. Human FOXP3+ T regulatory cell heterogeneity. *Clinical and Translational Immunology* **7**, 1–11 (2018).
33. Malhotra, N. *et al.* RORα-expressing T regulatory cells restrain allergic skin inflammation. *Science Immunology* **3**, 1–13 (2018).
34. Wohlfert, E. A. *et al.* GATA3 controls Foxp3 + regulatory T cell fate during inflammation in mice. *The journal of clinical investigation* **121**, 4503–4515 (2011).
35. Guo, X. *et al.* Global characterization of T cells in non-small-cell lung cancer by single-cell sequencing. *Nature medicine* **24**, 978–985 (2018).
36. Li, H. *et al.* Dysfunctional CD8 T Cells Form a Proliferative, Dynamically Regulated Compartment within Human Melanoma. *Cell* 1–15 (2018) doi:10.1016/j.cell.2018.11.043.
37. Wherry, E. J. & Kurachi, M. Molecular and cellular insights into T cell exhaustion. *Nature Reviews Immunology* **15**, 486–499 (2015).
38. van Duijn, J. *et al.* CD39 identifies a microenvironment-specific anti-inflammatory CD8 + T-cell population in atherosclerotic lesions. *Atherosclerosis* **285**, 71–78 (2019).
39. Chyu, K. Y. *et al.* CD8 + T cells mediate the athero-protective effect of immunization with an ApoB-100 peptide. *PLoS ONE* **7**, (2012).
40. Dwyer, D. F., Barrett, N. A., Austen, K. F., Immunological, T. & Consortium, G. P. Expression profiling of constitutive mast cells reveals a unique identity within the immune system. *Nature Immunology* **17**, 878–887 (2016).
41. Kapoor, N. *et al.* Transcription Factors STAT6 and KLF4 Implement Macrophage Polarization via the Dual Catalytic Powers of MCPIP. *The Journal of Immunology* **194**, 6011–6023 (2015).
42. Westerterp, M. *et al.* ATP-binding cassette transporters, atherosclerosis, and inflammation. *Circulation Research* **114**, 157–170 (2014).
43. Collot-Teixeira, S., Martin, J., McDermott-Roe, C., Poston, R. & McGregor, J. L. CD36 and macrophages in atherosclerosis. *Cardiovascular Research* **75**, 468–477 (2007).

44. Ramachandran, P. *et al. Resolving the fibrotic niche of human liver cirrhosis at single-cell level*. *Nature* vol. 575 (Springer US, 2019).
45. Jaitin, D. A. *et al.* Lipid-Associated Macrophages Control Metabolic Homeostasis in a Trem2-Dependent Manner. *Cell* **178**, 686-698.e14 (2019).
46. T, K., KHM, P., CK, G. & MPJ, de W. Transcriptional and epigenetic regulation of macrophages in atherosclerosis. *Nature Reviews Cardiology* (2019).
47. Wang, Z., Wang, D. Z., Pipes, G. C. T. & Olson, E. N. Myocardin is a master regulator of smooth muscle gene expression. *Proceedings of the National Academy of Sciences of the United States of America* **100**, 7129–7134 (2003).
48. Boltjes, A. & van Wijk, F. Human dendritic cell functional specialization in steady-state and inflammation. *Frontiers in Immunology* **5**, 1–13 (2014).
49. Villlani;, A.-C. *et al.* Single-cell RNA-Seq reveals new types of human blood dendritic cells, monocytes, and progenitors. *Science* **356**, (2017).
50. Efremova, M., Vento-Tormo, M., Teichmann, S. A. & Vento-Tormo, R. CellPhoneDB v2.0: Inferring cell-cell communication from combined expression of multi-subunit receptor-ligand complexes. *bioRxiv* 680926 (2019) doi:10.1101/680926.
51. Bonecchi, R. & Graham, G. J. Atypical Chemokine Receptors and Their Roles in the Resolution of the Inflammatory Response. *Frontiers in Immunology* **7**, (2016).
52. Engelbertsen, D. *et al.* Increased lymphocyte activation and atherosclerosis in CD47-deficient mice. *Scientific Reports* **9**, 1–12 (2019).
53. Sato, N. *et al.* Platelet-derived growth factor indirectly stimulates angiogenesis in vitro. *The American Journal of Pathology* **142**, 1119 (1993).
54. Corliss, B. A., Azimi, M. S., Munson, J., Peirce, S. M. & Murfee, W. L. Macrophages: An Inflammatory Link between Angiogenesis and Lymphangiogenesis. *Microcirculation (New York, N.Y. : 1994)* **23**, 95 (2016).
55. Lou, L., Zhang, P., Piao, R. & Wang, Y. Salmonella Pathogenicity Island 1 (SPI-1) and Its Complex Regulatory Network. *Frontiers in Cellular and Infection Microbiology* **9**, 270 (2019).
56. Cauchy, P. *et al.* Dynamic recruitment of Ets1 to both nucleosome-occupied and -depleted enhancer regions mediates a transcriptional program switch during early T-cell differentiation. *Nucleic Acids Research* **44**, 3567–3585 (2016).
57. Collin, M. & Bigley, V. Human dendritic cell subsets: an update. *Immunology* **154**, 3–20 (2018).
58. Akdis, M. *et al.* Interleukins (from IL-1 to IL-38), interferons, transforming growth factor β, and TNF-α: Receptors, functions, and roles in diseases. *Journal of Allergy and Clinical Immunology* **138**, 984–1010 (2016).
59. Hauer, A. D. *et al.* Blockade of interleukin-12 function by protein vaccination attenuates atherosclerosis. *Circulation* **112**, 1054–1062 (2005).
60. Tian, Y. *et al.* Unique phenotypes and clonal expansions of human CD4 effector memory T cells re-expressing CD45RA. *Nature Communications* **8**, (2017).
61. Mucida, D. *et al.* Transcriptional reprogramming of mature CD4 + helper T cells generates distinct MHC class II-restricted cytotoxic T lymphocytes. *Nature Immunology* **14**, 281–289 (2013).
62. Tian, Y., Sette, A. & Weiskopf, D. Cytotoxic CD4 T cells: Differentiation, function, and application to dengue virus infection. *Frontiers in Immunology* **7**, 531 (2016).
63. Reis, B. S., Rogoz, A., Costa-Pinto, F. A., Taniuchi, I. & Mucida, D. Mutual expression of the transcription factors Runx3 and ThPOK regulates intestinal CD4 + T cell immunity. *Nature Immunology* **14**, 271–280 (2013).

64. Kurachi, M. *et al.* The transcription factor BATF operates as an essential differentiation checkpoint in early effector CD8 + T cells. *Nature Immunology* **15**, 373–383 (2014).
65. Hoeksema, M. A., Stöger, J. L. & De Winther, M. P. J. Molecular pathways regulating macrophage polarization: Implications for atherosclerosis. *Current Atherosclerosis Reports* **14**, 254–263 (2012).
66. Goossens, P. *et al.* Myeloid type I interferon signaling promotes atherosclerosis by stimulating macrophage recruitment to lesions. *Cell Metabolism* **12**, 142–153 (2010).
67. Minematsu, H. *et al.* Nuclear presence of nuclear factor of activated T cells (NFAT) c3 and c4 is required for Toll-like receptor-activated innate inflammatory response of monocytes/macrophages. *Cellular Signalling* **23**, 1785–1793 (2011).
68. Fric, J. *et al.* NFAT control of innate immunity. *Blood* **120**, 1380–1389 (2012).
69. Kapoor, N. *et al.* Transcription factors STAT6 and KLF4 implement macrophage polarization via the dual catalytic powers of MCPIP. *Journal of Immunology* **194**, 6011–6023 (2015).
70. Erdmann, J., Kessler, T., Munoz Venegas, L. & Schunkert, H. A decade of genome-wide association studies for coronary artery disease: The challenges ahead. *Cardiovascular Research* **114**, 1241–1257 (2018).
71. Nelson, C. P. *et al.* Association analyses based on false discovery rate implicate new loci for coronary artery disease. *Nature Genetics* **49**, 1385–1391 (2017).
72. Van Dijk, R. A. *et al.* A Change in Inflammatory Footprint Precedes Plaque Instability: A Systematic Evaluation of Cellular Aspects of the Adaptive Immune Response in Human Atherosclerosis. doi:10.1161/JAHA.114.001403.
73. van Dijk, R. A., Virmani, R., von der Thüsen, J. H., Schaapherder, A. F. & Lindeman, J. H. N. The natural history of aortic atherosclerosis: a systematic histopathological evaluation of the peri-renal region. *Atherosclerosis* **210**, 100–6 (2010).
74. Téo, F. H. *et al.* Characterization of CD4+CD28null T cells in patients with coronary artery disease and individuals with risk factors for atherosclerosis. *Cell Immunol* **281**, 11–19 (2013).
75. Mosser, D. M. & Edwards, J. P. Exploring the full spectrum of macrophage activation. *Nature Reviews Immunology* **8**, 958–969 (2008).
76. Peeters, W. *et al.* Carotid atherosclerotic plaques stabilize after stroke insights into the natural process of atherosclerotic plaque stabilization. *Arteriosclerosis, Thrombosis, and Vascular Biology* **29**, 128–133 (2009).
77. Scholtes, V. P. W. *et al.* Type 2 diabetes is not associated with an altered plaque phenotype among patients undergoing carotid revascularization. A histological analysis of 1455 carotid plaques. *Atherosclerosis* **235**, 418–423 (2014).
78. Van Vré, E. A., Van Brussel, I., Bosmans, J. M., Vrints, C. J. & Bult, H. Dendritic cells in human atherosclerosis: from circulation to atherosclerotic plaques. *Mediators of inflammation* **2011**, 941396 (2011).
79. Villlani;, A.-C. *et al.* Single-cell RNA-Seq reveals new types of human blood dendritic cells, monocytes, and progenitors. *Science* **356**, (2017).
80. Howell, K. W. *et al.* Toll-like Receptor 4 Mediates Oxidized LDL-Induced Macrophage Differentiation to Foam Cells. *Journal of Surgical Research* **171**, e27–e31 (2011).
81. Karasawa, T. & Takahashi, M. Role of NLRP3 Inflammasomes in Atherosclerosis. *J Atheroscler Thromb* **24**, 443–451 (2017).
82. Ridker, P. M. *et al.* Antiinflammatory Therapy with Canakinumab for Atherosclerotic Disease. *New England Journal of Medicine* **377**, 1119–1132 (2017).

83. Buono, C. *et al.* Influence of interferon-γ on the extent and phenotype of diet-induced atherosclerosis in the LDLR-deficient mouse. *Arterioscler Thromb Vasc Biol* **23**, 454–460 (2003).
84. Gupta, S. *et al.* IFN-γ potentiates atherosclerosis in ApoE knock-out mice. *Journal of Clinical Investigation* **99**, 2752–2761 (1997).
85. Jessup, W., Gelissen, I. C., Gaus, K. & Kritharides, L. Roles of ATP binding cassette transporters A1 and G1, scavenger receptor BI and membrane lipid domains in cholesterol export from macrophages. *Current opinion in Lipidology* **17**, 247–257 (2006).
86. Tangirala, R. K. *et al.* Identification of macrophage liver X receptors as inhibitors of atherosclerosis. *Proc Natl Acad Sci U S A* **99**, 11896–11901 (2002).
87. Choi, S.-H. *et al.* Lipoprotein accumulation in macrophages via toll-like receptor-4-dependent fluid phase uptake. *Circulation research* **104**, 1355–63 (2009).
88. Xu, X. H. *et al.* Toll-like receptor-4 is expressed by macrophages in murine and human lipid-rich atherosclerotic plaques and upregulated by oxidized LDL. *Circulation* **104**, 3103–8 (2001).
89. Stewart, C. R. *et al.* CD36 ligands promote sterile inflammation through assembly of a Toll-like receptor 4 and 6 heterodimer. *Nature Immunology* **11**, 155–161 (2010).
90. Chou, M. Y. *et al.* Oxidation-specific epitopes are important targets of innate immunity. in *Journal of Internal Medicine* vol. 263 479–488 (John Wiley & Sons, Ltd, 2008).
91. Michelsen, K. S. *et al.* Lack of toll-like receptor 4 or myeloid differentiation factor 88 reduces atherosclerosis and alters plaque phenotype in mice deficient in apolipoprotein E. *Proceedings of the National Academy of Sciences of the United States of America* **101**, 10679–10684 (2004).
92. Monaco, C. *et al.* Toll-like receptor-2 mediates inflammation and matrix degradation in human atherosclerosis. *Circulation* **120**, 2462–9 (2009).
93. Duewell, P. *et al.* NLRP3 inflammasomes are required for atherogenesis and activated by cholesterol crystals. *Nature* **464**, 1357–1361 (2010).
94. Spann, N. J. *et al.* Regulated accumulation of desmosterol integrates macrophage lipid metabolism and inflammatory responses. *Cell* **151**, 138–152 (2012).
95. Baardman, J. *et al.* A Defective Pentose Phosphate Pathway Reduces Inflammatory Macrophage Responses during Hypercholesterolemia. *Cell Reports* **25**, 2044-2052.e5 (2018).
96. Neele, A. E. *et al.* Macrophage Kdm6b controls the pro-fibrotic transcriptome signature of foam cells. *Epigenomics* **9**, (2017).
97. Wesseling, M., Sakkers, T. R., de Jager, S. C. A., Pasterkamp, G. & Goumans, M. J. The morphological and molecular mechanisms of epithelial/endothelial-to-mesenchymal transition and its involvement in atherosclerosis. *Vascular Pharmacology* vol. 106 1–8 Preprint at https://doi.org/10.1016/j.vph.2018.02.006 (2018).
98. Cho, J. G., Lee, A., Chang, W., Lee, M.-S. & Kim, J. Endothelial to Mesenchymal Transition Represents a Key Link in the Interaction between Inflammation and Endothelial Dysfunction. *Frontiers in Immunology* **9**, 294 (2018).
99. Chen, P. Y. *et al.* Endothelial-to-mesenchymal transition drives atherosclerosis progression. *Journal of Clinical Investigation* **125**, 4514–4528 (2015).
100. Boyle, E. A., Li, Y. I. & Pritchard, J. K. An Expanded View of Complex Traits: From Polygenic to Omnigenic. *Cell* vol. 169 1177–1186 Preprint at https://doi.org/10.1016/j.cell.2017.05.038 (2017).
101. Verhoeven, B. A. N. *et al.* Athero-express: Differential atherosclerotic plaque expression of mRNA and protein in relation to cardiovascular events and patient characteristics. Rationale and design. *Eur J Epidemiol* **19**, 1127–1133 (2004).
102. Hellings, W. E. *et al.* Histological characterization of restenotic carotid plaques in relation to recurrence interval and clinical presentation: a cohort study. *Stroke* **39**, 1029–32 (2008).

103. Hashimshony, T. *et al*. CEL-Seq2: sensitive highly-multiplexed single-cell RNA-Seq. *Genome Biology* **17**, 77 (2016).
104. Li, H. & Durbin, R. Fast and accurate long-read alignment with Burrows-Wheeler transform. *Bioinformatics* **26**, 589–595 (2010).
105. Muraro, M. J. *et al*. A Single-Cell Transcriptome Atlas of the Human Pancreas. *Cell Systems* **3**, 385-394.e3 (2016).
106. R Core Team. R: A language and environment for statistical computing. https://www.r-project.org/ (2019).
107. Butler, A., Hoffman, P., Smibert, P., Papalexi, E. & Satija, R. Integrating single-cell transcriptomic data across different conditions , technologies , and species. *Nature Biotechnology* **36**, 411–420 (2018).
108. Martens, J. H. A. & Stunnenberg, H. G. BLUEPRINT: mapping human blood cell epigenomes. *Haematologica* **98**, 1487–1489 (2013).
109. Stuart, T. *et al*. Comprehensive Integration of Single-Cell Data. *Cell* **177**, 1888-1902.e21 (2019).
110. Schep, A. N., Wu, B., Buenrostro, J. D. & Greenleaf, W. J. ChromVAR: Inferring transcription-factor-associated accessibility from single-cell epigenomic data. *Nature Methods* **14**, 975–978 (2017).
111. Khan, A. *et al*. JASPAR 2018: Update of the open-access database of transcription factor binding profiles and its web framework. *Nucleic Acids Research* **46**, D260–D266 (2018).
112. Watanabe, K., Taskesen, E., van Bochoven, A. & Posthuma, D. Functional mapping and annotation of genetic associations with FUMA. *Nature communicationsommunications* **8**, 1–11 (2017).
113. Auton, A. *et al*. A global reference for human genetic variation. *Nature* vol. 526 68–74 Preprint at https://doi.org/10.1038/nature15393 (2015).
114. de Leeuw, C. A., Mooij, J. M., Heskes, T. & Posthuma, D. MAGMA: Generalized Gene-Set Analysis of GWAS Data. *PLoS Computational Biology* **11**, e1004219 (2015).

Online Data supplement

Expanded materials and methods

Patient population

Atherosclerotic plaques were obtained from 14 male and 4 female patients undergoing a carotid endarterectomy (CEA) procedure. All plaque specimens were included in the Athero-Express Biobank Study (AE, www.atheroexpress.nl), an ongoing biobank study at the University Medical Centre Utrecht (UMCU)[101] (Cohort 1). Only primary CEAs were included, restenotic plaques were excluded due to their difference in composition compared to primary atherosclerotic plaques[102]. The study was approved by the Medical Ethical Committee of the UMCU. For flow cytometry, seven plaques (5 male, 2 female) were used that were obtained from patients undergoing CEA procedure at Haaglanden Medical Center Westeinde (The Hague, The Netherlands) (Cohort 2). The study was approved by the Medical Ethical Committee of the HMC. For scATAC-Seq, atherosclerotic plaque samples were obtained from 3 patients undergoing CEA procedure at Kuopio University Hospital, Kuopio, Finland (Cohort 3). The studies were approved by Local Ethical Committee of Kuopio University Hospital. All studies were performed in accordance with the declaration of Helsinki and all patients gave written informed consent before start of the study.

Human plaque processing (Single Cell)

Human carotid plaques of Cohort 1 were collected during CEA; the culprit segment (5 mm) was used for histology and embedded in paraffin as described elsewhere[101]. Time between surgical removal and plaque processing did not exceed 10 minutes. The inclusion of a small medial layer in the dissected tissue could not be excluded during the surgical procedure. The plaques were characterized as fibrous (n = 6), fibro-atheromatous (n = 6) or atheromatous (n = 6). Characterization was in concordance with the Athero-Express Biobank Study protocols. The remainder of the plaque washed in RPMI and minced into small pieces with a razor blade. The tissue was then digested in RPMI 1640 containing 2.5 mg/mL Collagenase IV (ThermoFisher Scientific), 0.25 mg/mL DNAse I (Sigma), 2.5 mg/mL Human Albumin Fraction V (MP Biomedicals) and 1 mM Flavopiridol (Selleckchem) at 37°C for 30 minutes. Subsequently, the plaque cell suspension was filtered through a 70 µm cell strainer and washed with RPMI 1640. Cells were kept in RPMI 1640 with 1% Fetal Calf Serum until subsequent staining for fluorescence-activated cell sorting. Remaining, unstained cells were cryostored in liquid nitrogen.

Immunohistochemistry

Immunohistochemical staining of CD3, CD34, αSMA (ACTA2) and CD68 was performed fully automated (Benchmark, Ventana Medical Systems, Yuscon AZ). Stainings were performed on matched samples of patients from cohort 1 (n = 3). The CD3 antibody was purchased from DAKO and used at a dilution of 1:100. The CD68 antibody was purchased from Novocastra (cat. No. NCL-CD68-KP1) and used at a dilution of 1:3200. The CD34 antibody was purchased from Ventana Medical Systems (cat. No. 790-2927) and used at the dilution recommended by manufacturer. The αSMA antibody was purchased from Sigma (cat. No. A2547) and used at a dilution of 1:20000.

Human plaque processing (whole tissue)

Whole plaque tissue RNA-seq was obtained from two male Athero-Express biobank samples. RNA-seq library preparation was performed using the CEL-Seq2 Sample Preparation Protocol[103] and sequenced as 2 x 75bp paired-end on a Illumina NextSeq 500 (Utrecht Sequencing Facility). The reads were de-multiplexed and aligned to human cDNA reference using the BWA (v0.7.13)[104]. Downstream analysis was performed using custom R scripts.

Fluorescent activated cell sorting of viable cells

Single cell suspensions were stained with Calcein AM and Hoechst (ThermoFisher Scientific) in PBS supplemented with 5% Fetal Bovine Serum (FBS) and 0.2% ethylenediaminetetraacetic acid (EDTA) for 30 minutes at 37°C. After staining, cells were washed and filtered through a 70 μm FlowMi cell strainer (SP Scienceware). Viable cells, positive for both Calcein AM and Hoechst, were sorted using the Beckman Coulter MoFlo Astrios EQ.

Flow cytometry

Flow cytometry was performed on defrosted single cell suspensions of plaques from three patients of cohort 1 and on seven plaques single cell suspensions from cohort 2 (characterized as advanced plaques that showed luminal thrombosis, regions of intraplaque hemorrhage, large macrophage regions and a large necrotic core). All samples were digested according to the same protocol as described above for the scRNA-seq samples. The single plaque cells were stimulated with phorbol 12-myristate 13-acetate (PMA, 50 ng/mL, Sigma-Aldrich), ionomycin (500 ng/mL, Sigma-Aldrich) and Brefeldin A (ThermoFisher Scientific) for 3.5h in complete RPMI at 37°C and 5% CO_2. Subsequently, cells were stained with extracellular antibodies, fixated, permeabilized and stained with intracellular antibodies **(Online Table 4**). The fluorescently labeled plaque cells were measured using a Cytoflex S (Beckman

and Coulter) and analysed with FlowJo software. Statistical analysis was performed using Graphpad Prism 8 software. Data passed the Shapiro-Wilk normality test and an unpaired T-test was performed to determine significance.

Single cell RNA-sequencing

Using a Mosquito® HTS (TTP Labtech) 384 wells plates were filled with 50nL lysis buffer containing CELseq2-primers, spike-ins and dinucleotide triphosphates (dNTPs) and overlaid with mineral oil to prevent evaporation. Viable cells were sorted one cell per well into these 384 wells plates, fixed by lysis to preserve expression status, and immediately frozen at -80°C until further processing. First, cDNA was constructed using the SORT-seq protocol[105]. In short, cells were lysed for 5 min at 65°C and subsequently reverse transcription and second strand mixes were added using the Nanodrop II liquid handling platform (GC biotech). Next, cells were pooled in one library and the aqueous phase was separated from the oil phase, followed by in vitro transcription (IVT). A library was formed using the CEL-Seq2 protocol[103]. Primers consisted of a 24 bp polyT stretch, a 64bp random molecular barcode (UMI), a cell-specific 8bp barcode, the 5' Illumina TruSeq small RNA kit adaptor and a T7 promoter. For sequencing, TruSeq small RNA primers (Illumina) were added to the libraries and sequenced paired end at 75 bp read length using Illumina NextSeq 500.

scRNA-seq data processing and clustering

Single-cell sequencing data were processed as described previously[105]. Analyses were performed in an R 3.5 environment[106] using Seurat (version 2.3.4 and 3.0)[107]. Prior to processing, reads were filtered for mitochondrial and ribosomal genes, MALAT1, KCNQ1OT1, UGDH-AS1, and EEF1A. In order to omit doublets and low-quality cells, only cells expressing between 500 and 10.000 genes and genes expressed in at least 3 cells were used for further analysis. The following steps were performed using Seurat (version 2.3.4): data was log-normalized and scaled with the exclusion of unique molecular identifiers (UMIs). Top variable genes for all samples were used to combine samples into one object using Seurat function RunMultiCCA(), after which samples were aligned using AlignSubspace() with reduction.type=CCA and grouping.var="plate". Subsequently, canonical correlation analysis (CCA) reduction was performed with a resolution of 1.2 for 15 dimensions to identify clusters and to perform t-distributed stochastic neighbor embedding (tSNE). Cell types were assigned to cell clusters by evaluating gene expression of individual cell clusters using differential gene expression (Wilcoxon rank sum test) and analysis with SingleR[8] against BLUEPRINT[108] reference data. Sub-clustering of identified cell clusters was performed using CCA with a resolution of 0.9 or 1.5 for 15 dimensions (Seurat version 2.3.4). Downstream analysis of initial and sub-clusters was performed in a similar manner. Pathway analysis were

performed using the EGSEA (version 1.16.0) with Canonical pathway and hallmark gene set collections from broad institute GSEA (version 1.17.0) and FDR for multiple testing correction. tSNE plots, dot plots and violin plots were made with Seurat (version 2.3.4 and 3.0). Figure 1E and S2C were made using SingleR (version 1.2.4). Barplots were made using ggplot2. For full details, see ***Data access.***

Comparison whole- tissue and single-cell RNA-seq

Ilumina cell sequencing data was processed as described previously[105]. In summary, prior to processing reads were filtered for mitochondrial and ribosomal genes, MALAT1, KCNQ1OT1, UGDH-AS1 and EEF1A, and duplicate or unannotated entries. A "pseudobulk" patient was created by combining reads from all patients. Individual patients and the pseudobulk patient were compared to bulk RNA-seq as described above. Correlation coefficient was determined through Pearson correlation (CI 0.95). Scatterplot was made using ggplot2. All processing was performed using custom R scripts. For full details, see ***Data access***.

Integration of mouse datasets

Top 20 marker genes from all myeloid cell clusters in the 4 mouse datasets[3–6] were converted to human symbols using the ENSEMBL biomaRt R package (v2.42.0) in an R v3.5.3 environment. Subsequently, the overlap of genes in the mouse clusters with significant (p.adj < 0.1) marker genes from My.0, My.1, and My.2 was determined and significance calculated by hypergeometric test using standard R function phyper() with parameters q-1 and lower.tail = F. Finally, bar graphs were generated with ggplot2 and circos plots of overlaps were generated on http://metascape.org by uploading lists of marker genes per cluster, starting a custom analysis, and downloading the corresponding 'gene circos.svg' file from the 'ID conversion' tab. For full details, see ***Data access***.

Ligand-receptor interaction analysis

Ligand-receptor interactions were calculated using cellphonedb [v2.11 – database version 2.0.0][50] with default settings. Heatmap was made with cellphonedb. Top significant ($p < 0.05$) interactions were defined as > 3rd quartile and plotted using ggplot2. For full details, see ***Data access***.

Human plaque processing for scATAC-Seq

The tissue samples from cohort 3 (characterized as fibro-atheromatous) were minced with a scalpel and enzymatically dissociated using Miltenyi Biotec Multi-Tissue Dissociation Kit supplemented with 0.5% BSA and 20 mM HEPES buffer (pH 7.2-7.5) for 60 min at 37 °C with end-over-end rotation. The suspension was passed through a 30 µm strainer and viable cells were purified magnetically using the Dead Cell Removal

Kit (Miltenyi Biotec). For the isolation of nuclei from cells, the lysis buffer formulation recommended by 10x Genomics for scATAC-Seq nuclei preparation was used. The nuclei were purified by iodixanol (OptiPrep; Sigma) density gradient centrifugation at 3300g for 20 min at 4 °C. The nuclei were recovered at the interface of 29% and 35% iodixanol. The nuclei were resuspended in ice-cold 10x Genomics Nuclei Buffer and counted using fluorescence staining (DAPI). Approximately 5000-6000 nuclei per sample were processed on the 10x Genomics Chromium Controller instrument, followed by scATAC-Seq library preparation according to the manufacturer's protocol. The libraries were sequenced on an Illumina NextSeq sequencer using the standard protocol recommended by 10x Genomics for scATAC-Seq libraries.

scATAC-Seq data analysis

Sequencing data preprocessing, library quality control, cell calling and peak calling were done with the Cell Ranger ATAC pipeline (10x Genomics, version 1.1). Integration of scATAC-Seq samples, clustering of cells, and visualization of chromatin accessibility and pseudobulk coverage tracks was performed with Seurat (version 3.0)[109] and its extension Signac (version 0.15; https://github.com/timoast/signac). scATAC-Seq cells were matched to scRNA-Seq cell types using the scRNA-Seq as the reference data set in a cross-modal label transfer procedure, as described in Stuart *et al*.(2019).[109] Differential motif accessibility was calculated using chromVAR (version 1.5)[110] using the human motifs from the JASPAR CORE motif collection (2018 release)[111]. First, at the level of individual cells, the relative accessibility of each motif genome-wide ('motif activity') was computed as the deviation in motif occurrence in the accessible peaks compared to a set of background peaks matched for GC content, using the default parameters of the chromVAR method.[110] Subsequently, cell clusters were tested for differences (both positive and negative direction) in motif activity using a logistic regression test with the total peak count as a latent variable, as suggested for differential motif analysis by the authors of the Signac package109. $P < 0.05$ after correction for multiple testing using the Benjamini–Hochberg procedure was considered significant. Heatmaps were made using pheatmap (version 1.0.12), genome plots were made using Signac. For full details, see ***Data access***.

Differential gene expression analysis and mapping of GWAS loci

For the analysis and mapping of CAD associated gene to the single-cell RNAseq data, we applied three steps: 1) we prioritized genes based on the CAD GWAS summary statistics, 2) we determined the genes differentially expressed between cell type and therefore specific to these cell types, and 3) we overlapped the GWAS-derived genes and differentially expressed genes to identify genes associated to CAD and specific to a cell type.

Step 1: We used the summary statistics from the GWAS on CAD by Nelson *et al.* which included CARDIoGRAMplusC4D and UK Biobank data[71]. This data was annotated with a the Functional Mapping and Annotation of Genome-Wide Association Studies (FUMA v1.3.3b, https://fuma.ctglab.nl) platform.[112] FUMA can be used to annotate, prioritize, visualize and interpret GWAS results. In short, FUMA takes GWAS summary statistics as an input, it will map and match the results to a reference (in this case the 1000G EUR population, https://www.internationalgenome.org[113]), and provides extensive functional annotation for all SNPs (present in the summary statistics and the reference used) in genomic areas identified by lead SNPs. Various filters can be applied. Here, we applied genome-wide significance ($p = 5x10^{-8}$), a linkage disequilibrium $r^2 = 0.05$ for clumping of independent loci within 1000 kb of the lead variant (PLINK version 1.9), and included only variants with minor allele frequency (MAF) > 1%. Annotation and mapping of genes were based on 1) position (within 1000kb of the lead variant), 2) limited to blood and vascular bed derived data from the Genotype-Tissue Expression (GTEx version 7) Project only. This resulted in a list of 644 genes that mapped to CAD loci. To further prioritize these 644 genes, we calculated per-gene p-values based on the per-SNP p-values from the CAD GWAS summary statistics. To this end FUMA uses MAGMA (https://ctg.cncr.nl/software/magma, v1.06[114]). MAGMA first analyses the individual SNPs in a gene and combines the resulting SNP p-values into a gene test-statistic while taking into account the underlying LD structure. Using permutations based on a randomly generated test-statistic drawn from the standard normal distribution, a per-gene empirical (permuted) p-value is derived. This results in a per-gene p-value of association with CAD for all genes in a reference (here ENSEMBL v92 was used and we only included protein-coding genes). We further prioritized the 644 genes mapped to CAD loci by selecting genes with a MAGMA p-value < 0.05. This selection resulted in 317 CAD associated genes (mapped to CAD associated loci) which were used for the downstream single-cell analysis and mapping.

Step 2: For the single-cell analysis and mapping, we have focused only on genes that 1) are specific for the different cell types in plaque, and that 2) have a genetic association with CAD. The purpose of the analysis is to find those genes in each cell type to provide tangible starting points for functional testing. Genes that are highly specific (i.e., highly expressed) are more likely to have a specific function within the cells, making them interesting targets when these genes are also genetically correlated with the disease. To this end we performed a differential gene expression analysis, resulting in 3876 differentially expressed genes (DEG) listed in figure 7A, the second pillar of this analysis. For better interpretation and visualization, we sorted these genes into 15 gene expression patterns, which highlight the expression of genes in specific (related) cell types. Differential expression was tested between clusters by

Wilcoxon sum rank testing in both a "One cluster vs. One cluster" and "One cluster vs. Remaining clusters" fashion. Genes were deemed differentially expressed if they met 2 criteria: 1) >= 10% of cells within one cell cluster express the gene with log2 fold change of >= 0.6, and 2) the gene passes the Bonferroni adjusted significance threshold of p.adjusted < 0.05 for this test. The 3876 differentially expressed genes (DEG) were sorted into 15 gene expression patterns by K-means clustering based on average expression per cell type (**Online Table 3**).

Step 3: After this, the 317 CAD associated genes derived from the GWAS summary statistics and the 3876 DEGs derived from the scRNAseq data are overlapped. This resulted in 74 genes that are both highly expressed in scRNAseq data (a DEG), and are associated to CAD based on GWAS summary statistics. We calculated enrichment of the 74 DEGs in the 15 gene expression patterns using permutation analysis. We sampled 75000 random sets of 317 genes from 26180 genes that were possible to map. We then calculated positive enrichment for each gene expression pattern for the mapped GWAS genes compared to the random sets and determined the enrichment of DEGs. Downstream processing was performed using custom R scripts. Heatmap was made with Seurat (version 2.3.4) and bar graph with ggplot2. For full details, see ***Data access***.

Data access

In silico data analysis was performed using custom R scripts (R version 3.5.3) designed especially for this research and/or based on the recommended pipelines from the pre-existing packages listed in the individual segments above. R scripts are available on GitHub [https://github.com/AtheroExpress/MicroanatomyHumanPlaque_scRNAseq] Other data is available upon personal request to the corresponding authors (m.mokry@umcutrecht.nl; j.kuiper@lacdr.leidenuniv.nl; m.dewinther@amsterdamumc.nl; g.pasterkamp@umcutrecht.nl).

Supplemental Tables

For supplemental tables see https://doi.org/10.1161/CIRCRESAHA.120.316770

Supplemental Figures

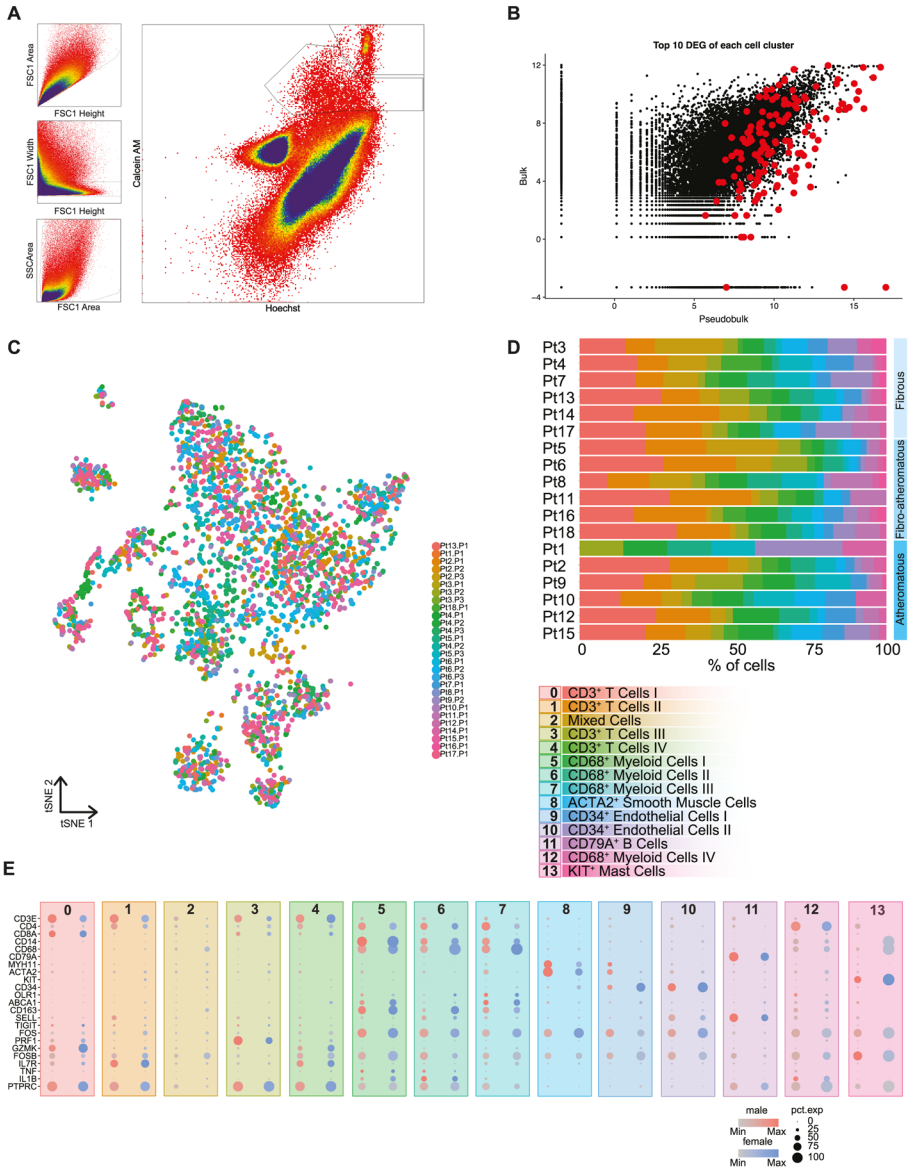

Online Figure 1. CCA clustering and tSNE visualization revealed 14 distinct populations. A) FACS plots showing gating directions for viable cells, positive for both Calcein AM and Hoechst B) Single cell CEL-seq2 libraries showed good correlation with plaque bulk RNA-seq libraries. Correlation 0.643 $p < 2.2e\text{-}10$. C) Clusters were not biased towards individual PCR plates or patients. D) Relative cluster sizes were comparable between patients. E) Dotplot of marker genes confirmed population identities and low inter-sex variance.

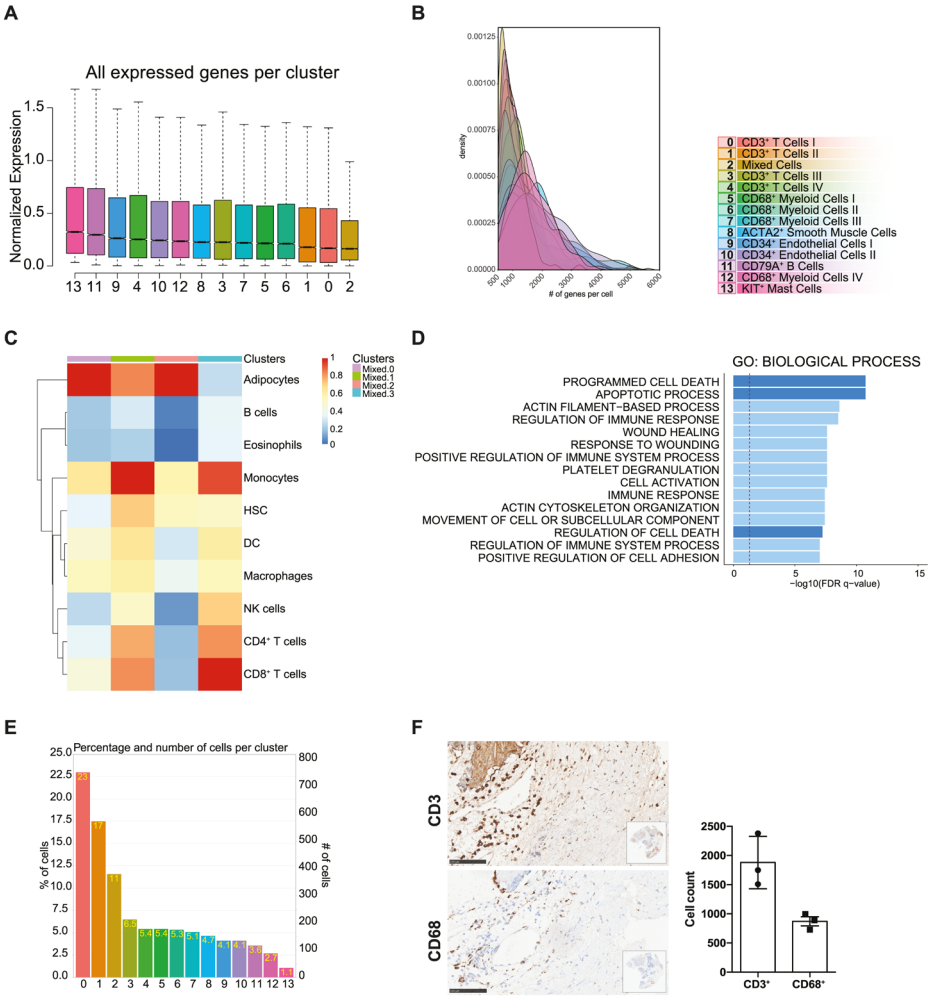

Online Figure 2. Refinement of population identities. A) Boxplots of normalized gene expression per cluster. B) Per cluster density plots of number of detected genes per cell. C) Heatmap of subclusters of unknown cluster 2's similarity to reference datasets of known cell types. D) Top pathways associated with cluster 2. E) Distribution of number of cells per cluster. F) Immunostaining of 3 representative endarterectomy samples. Top left: CD3$^+$ T cells. Bottom Left: CD68$^+$ macrophages. Right: Barplots of positive cell counts, data shown as mean±SD (n = 3). Scale bars represent 100µm.

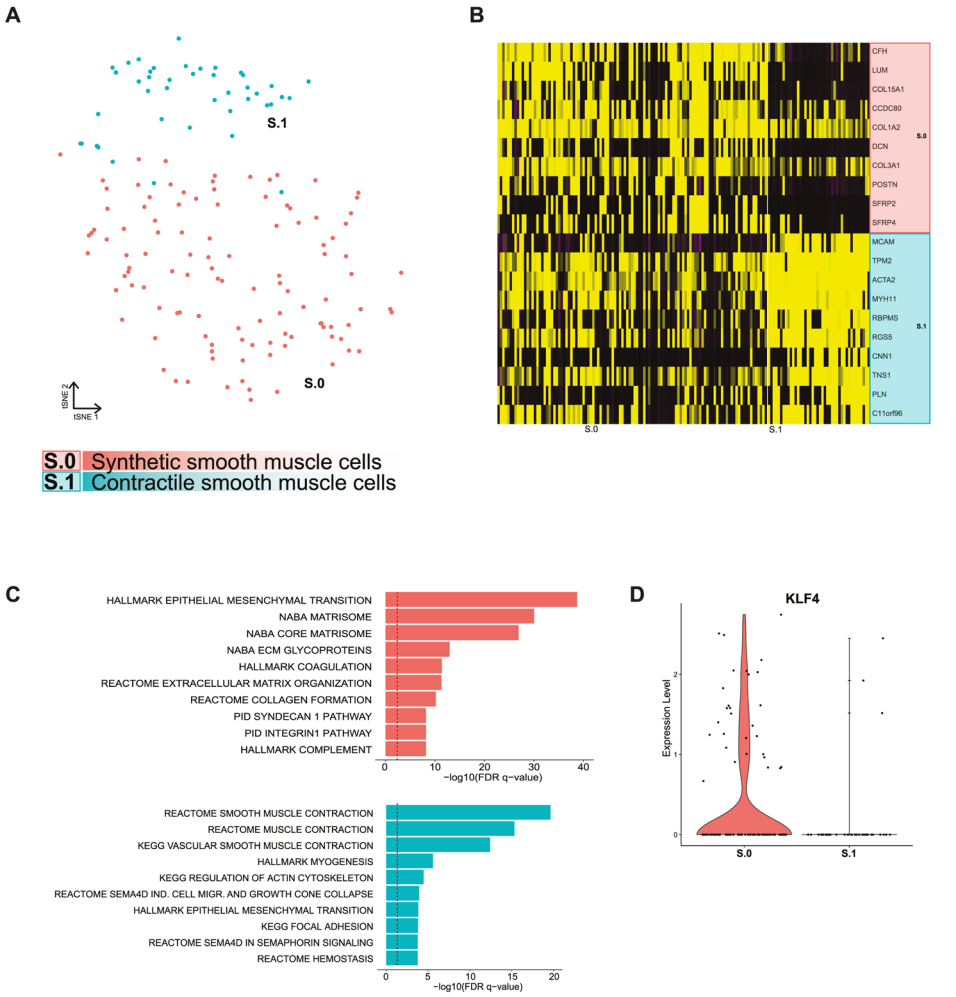

Online Figure 3. Subclustering of smooth muscle cells revealed 2 distinct populations. A) tSNE visualization of clustering revealed 2 distinct smooth muscle cell populations. B) Heatmap of top marker genes per cluster. C) Top pathways associated with each population.

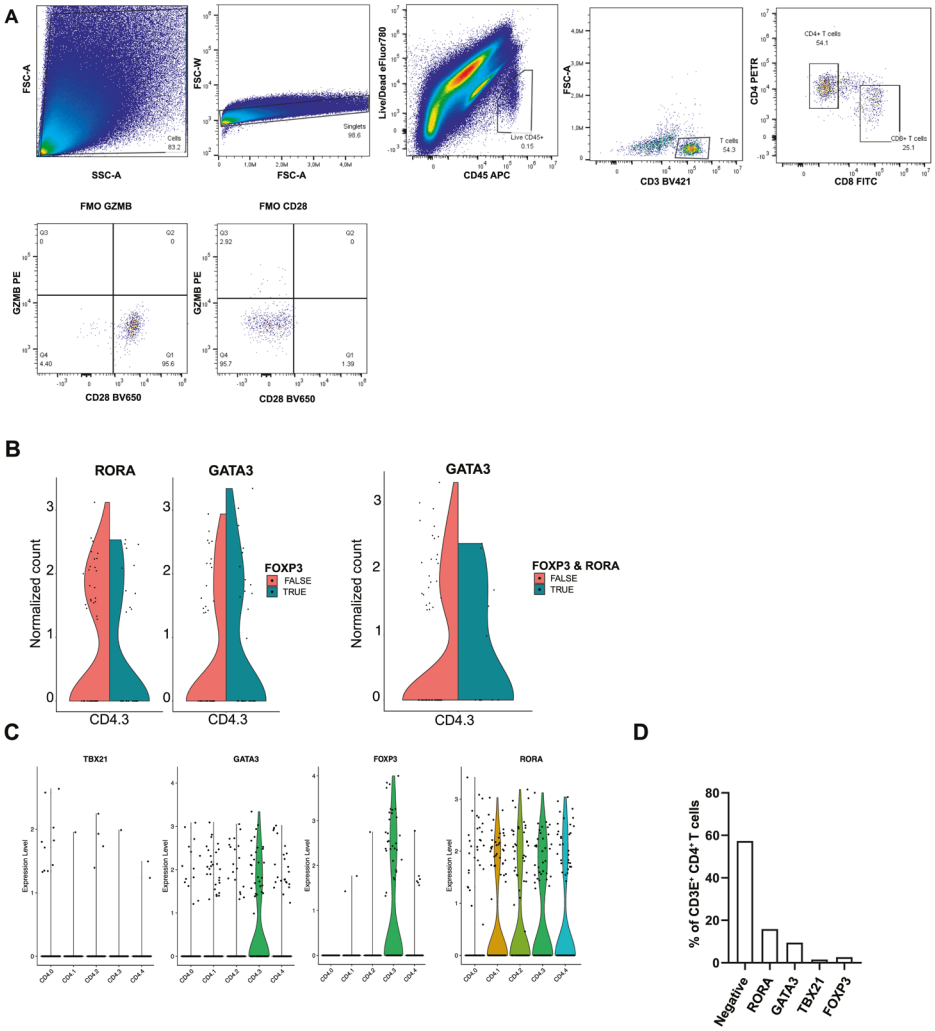

Online Figure 4. Representation of potential T_H-subsets in the human plaque. A) Gating strategy for GZMB staining within $CD4^+CD28^{null}$ T cells. B) Split-violins showing a correlation between expression of FOXP3 and respectively RORA and GATA3; and cells that express all three transcription factors. C) Violin plots showing expression of helper T cell subset-related transcription factors within the $CD4^+$cluters. D) Independent analysis of all $CD3E^+CD4^+$ T cells. Negative $CD4^+$ T cells are negative for all transcription factors. Other bars represent the percentage of $CD4^+$ T cells that specifically express the noted transcription factor. RORC was not detected in our dataset.

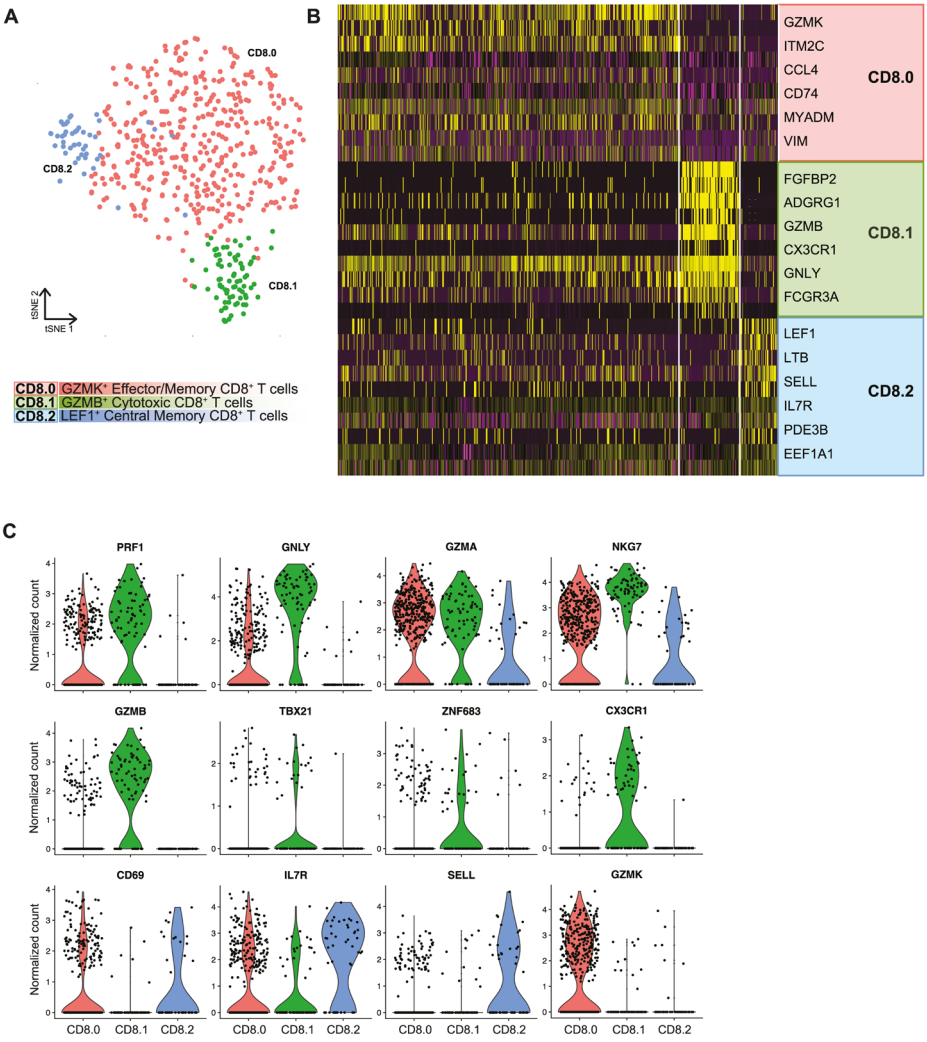

Online Figure 5. Subclustering of CD8⁺ T cells revealed 3 distinct populations. A) tSNE visualization of clustering revealed 4 distinct CD8⁺ T cell populations. B) Heatmap of top marker genes per cluster. C) Violin plots of marker genes associated with CD8⁺ T cell cytotoxicity and quiescence.

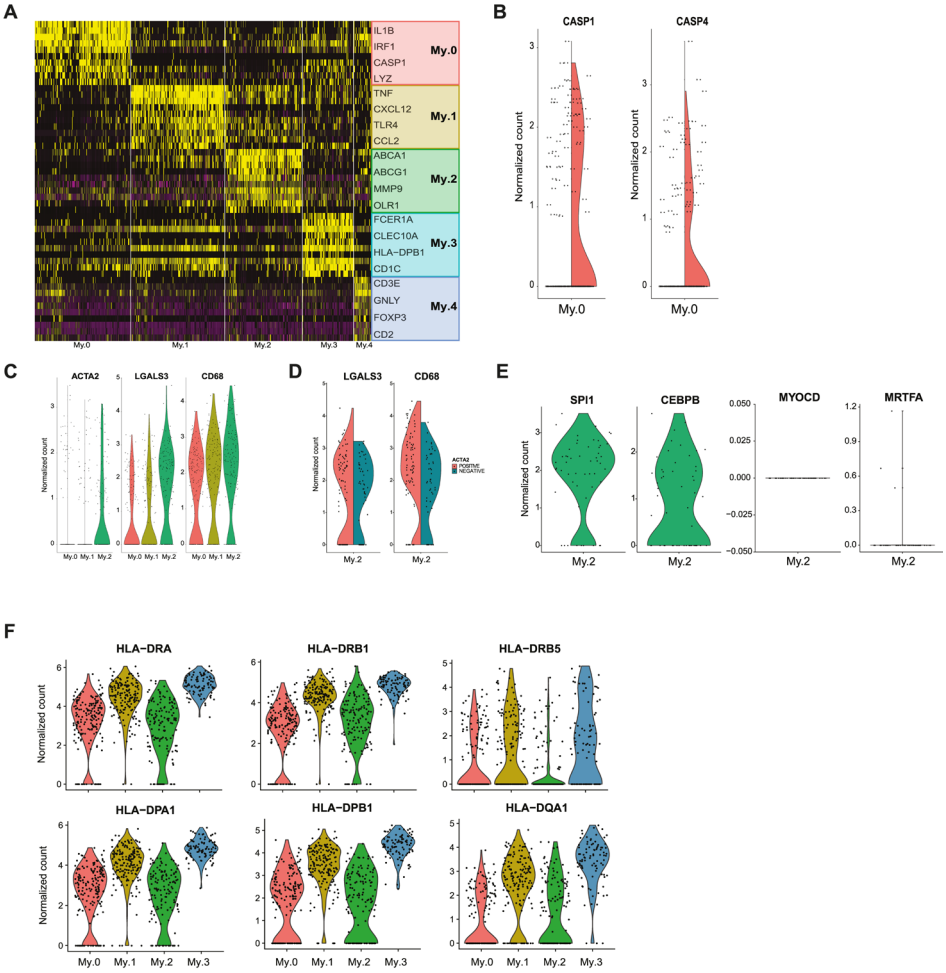

Online Figure 6. Myeloid population marker genes and SMC related gene expression. A) Heatmap of top marker genes per cluster. B) Split violin plot showing *CASP1* and *CASP4* expression in *IL1B*$^{-}$ (left side of violins) and *IL1B*$^{+}$ cells (right side of violins). C) Violin plot showing genes associated with the transition of smooth muscle cell to macrophage. D) Correlation of ACTA2 expression with CD68 and LGALS3 levels in cluster My.2. E) Violin plots of *ACTA2*$^{+}$ cells in cluster My.2 showing expression of myeloid lineage transcription factors *SPI1* and *CEBPB* and smooth muscle cell lineage transcription factors *MYOCD* and *MRTFA*. F) Violin plots of class II HLA subtypes expressed by cluster My.0 – My.4.

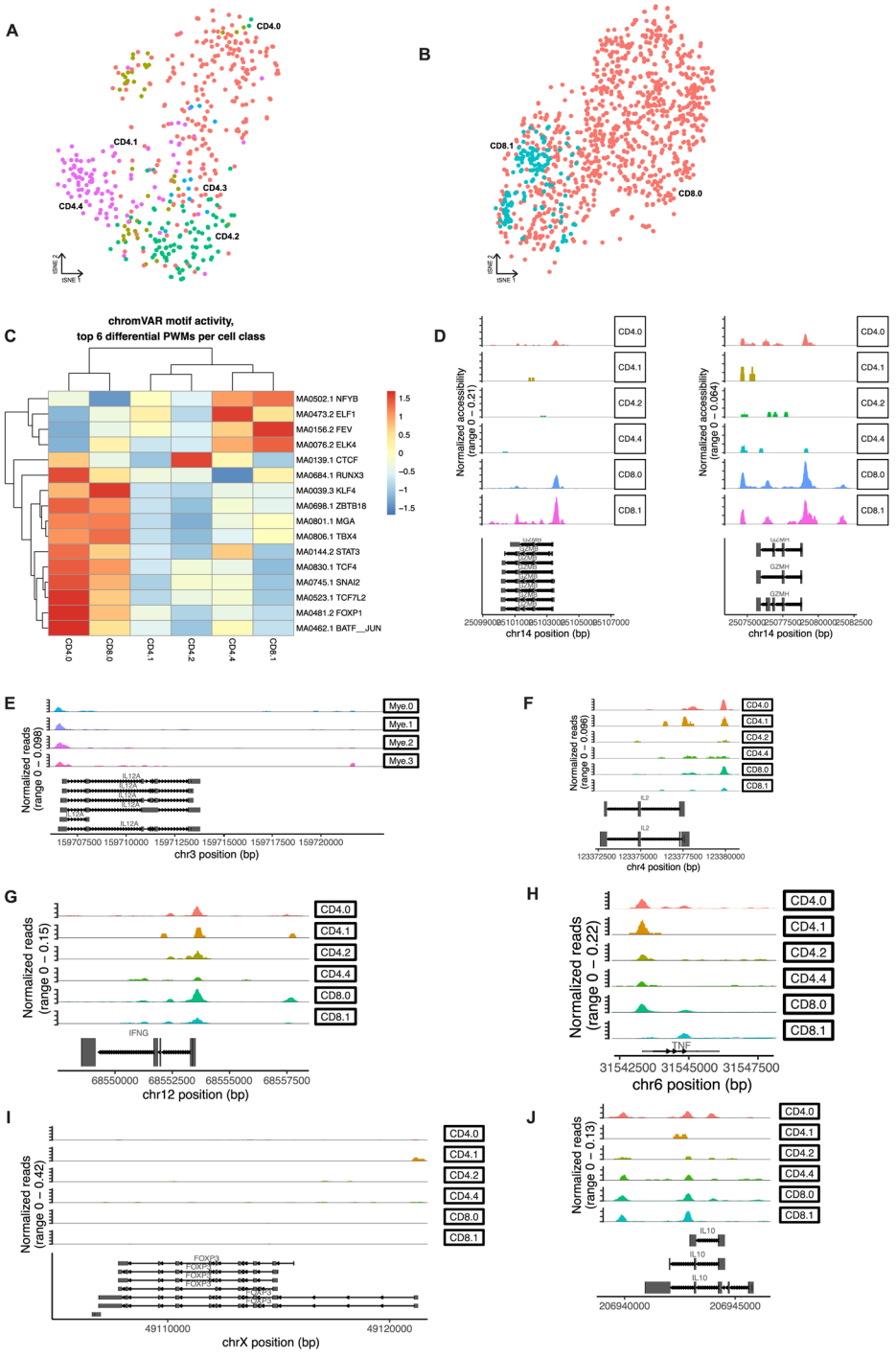
A
CD4.0
CD4.1
CD4.3
CD4.4
CD4.2
tSNE 2
tSNE 1
B
CD8.1
CD8.0
C
chromVAR motif activity,
top 6 differential PWMs per cell class
MA0502.1 NFYB
MA0473.2 ELF1
MA0156.2 FEV
MA0076.2 ELK4
MA0139.1 CTCF
MA0684.1 RUNX3
MA0039.3 KLF4
MA0698.1 ZBTB18
MA0801.1 MGA
MA0806.1 TBX4
MA0144.2 STAT3
MA0830.1 TCF4
MA0745.1 SNAI2
MA0523.1 TCF7L2
MA0481.2 FOXP1
MA0462.1 BATF::JUN
CD4.0
CD8.0
CD4.1
CD4.2
CD4.4
CD8.1
D
Normalized accessibility
(range 0 – 0.21)
Normalized accessibility
(range 0 – 0.064)
CD4.0
CD4.1
CD4.2
CD4.4
CD8.0
CD8.1
chr14 position (bp)
E
Normalized reads
(range 0 – 0.096)
Mye.0
Mye.1
Mye.2
Mye.3
IL12A
chr3 position (bp)
F
Normalized reads
(range 0 – 0.096)
IL2
chr4 position (bp)
G
Normalized reads
(range 0 – 0.15)
IFNG
chr12 position (bp)
H
Normalized reads
(range 0 – 0.22)
TNF
chr6 position (bp)
I
Normalized reads
(range 0 – 0.42)
FOXP3
chrX position (bp)
J
Normalized reads
(range 0 – 0.13)
IL10

◂ Online Figure 7. Chromatin accessibility of T cells in human atherosclerotic plaques analyzed using scATAC-seq. A) tSNE visualization of $CD4^+$ T cell subclusters. B) tSNE visualization of $CD8^+$ T cell subclusters. C) Heatmap showing the top differential TF motifs based on chromVAR. Pseudobulk genome browser visualization identifying the open chromatin regions of E) *IL12*, F) *IL2*, G) *IFNG*, H) *TNF*, I) *FOXP3* and J) *IL10*.

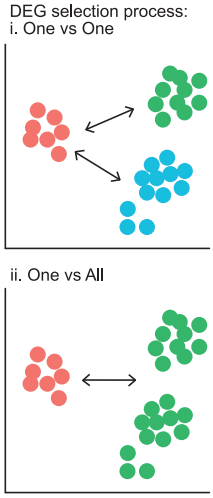

Online Figure 8. Projection of CAD GWAS associated genes: DEG selection process. Schematic overview of differentially expressed gene (DEG) selection. Top: DEG were called comparing all clusters against one another. Bottom: DEG were called comparing one cluster against all others aggregated.